Redox Biology 69 (2024) 103001

Contents lists available at ScienceDirect

Redox Biology

journal homepage: www.elsevier.com/locate/redox

Regulation of respiratory complex I assembly by FMN cofactor targeting

Andrea Curtabbi [a,b], Adela Guarás [a], José Luis Cabrera-Alarcón [a,b], Maribel Rivero [c,d], Enrique Calvo [a,e], Marina Rosa-Moreno [a], Jesús Vázquez [a,e], Milagros Medina [c,d], José Antonio Enríquez [a,b,*]

[a] Centro Nacional de Investigaciones Cardiovasculares Carlos III, Madrid, Spain
[b] CIBER de Fragilidad y Envejecimiento Saludable (CIBERFES), Madrid, Spain
[c] Departamento de Bioquímica y Biología Molecular y Celular, Facultad de Ciencias, Universidad de Zaragoza, Zaragoza, Spain
[d] Instituto de Biocomputación y Física de Sistemas Complejos (BIFI), Universidad de Zaragoza, Zaragoza, Spain
[e] CIBER de Enfermedades Cardiovasculares (CIBERCV), Madrid, Spain

ARTICLE INFO

Keywords:
Respiratory complex I
FMN
OXPHOS
DPI

ABSTRACT

Respiratory complex I plays a crucial role in the mitochondrial electron transport chain and shows promise as a therapeutic target for various human diseases. While most studies focus on inhibiting complex I at the Q-site, little is known about inhibitors targeting other sites within the complex. In this study, we demonstrate that diphenyleneiodonium (DPI), a *N*-site inhibitor, uniquely affects the stability of complex I by reacting with its flavin cofactor FMN. Treatment with DPI blocks the final stage of complex I assembly, leading to the complete and reversible degradation of complex I in different cellular models. Growing cells in medium lacking the FMN precursor riboflavin or knocking out the mitochondrial flavin carrier gene SLC25A32 results in a similar complex I degradation. Overall, our findings establish a direct connection between mitochondrial flavin homeostasis and complex I stability and assembly, paving the way for novel pharmacological strategies to regulate respiratory complex I.

1. Introduction

In recent years, the involvement of respiratory complex I in the development of various common human diseases has become evident. Extensive research is currently underway to investigate drugs that target complex I as potential treatments for conditions such as ischemia reperfusion injury [1] and cancer [2]. Most drugs under study are active at the Q-site, which is the binding site for quinone molecules in the enzyme [3–5]. However, an alternative druggable site within complex I is the flavin mononucleotide (FMN) prosthetic group, which is known as the *N*-site due to its NADH-oxidizing activity. The reactivity of the *N*-site FMN has been extensively studied [6], and its potential role as a source of reactive oxygen species (ROS) in both normal physiological processes and disease has attracted considerable attention in recent years [7,8]. Nevertheless, due to the limited availability of *N*-site inhibitors, there are still crucial aspects of complex I FMN biology that remain unexplored.

Flavin cofactors are essential partners in numerous biological redox reactions [9], and compounds derived from riboflavin are present in all living organisms. Besides complex I, several other mitochondrial enzymes also rely on flavin cofactors for their activity [10]. However, the specific enzymes and transporters responsible for the uptake and conversion of riboflavin into FMN and FAD within mitochondria are still a subject of debate [11]. Additionally, despite significant progress in understanding the intricated assembly pathway of complex I, the mechanism by which FMN is inserted into the enzyme remains unknown [12].

In yeast, even a single amino acid substitution within the FMN binding pocket of the NDUFV1 subunit of complex I is enough to cause the complete loss of complex I [13]. In humans, the notion that riboflavin may play a role in regulating and enhancing complex I activity has led to the use of riboflavin supplementation as a treatment for complex I deficiency. This approach has shown varying degrees of symptom improvement in some patients [14–16]. Whether the stability of mammalian complex I is regulated by its flavin cofactor, as it is the case for many other flavoenzymes [17–19], is yet unexplored.

To address these unresolved questions, we conducted a study focusing on the biology of complex I inhibition using diphenyleneiodonium (DPI), a well-known *N*-site inhibitor. DPI functions by

* Corresponding author. Centro Nacional de Investigaciones Cardiovasculares Carlos III, Madrid, Spain.
E-mail address: jaenriquez@cnic.es (J.A. Enríquez).

https://doi.org/10.1016/j.redox.2023.103001
Received 18 September 2023; Received in revised form 5 December 2023; Accepted 14 December 2023
Available online 20 December 2023

covalently reacting with the reduced FMN cofactor, thereby irreversibly blocking electron input into the enzyme [20]. Our investigation revealed that sequestration of FMN by DPI has a profound effect on the stability of complex I. In the absence of a functional FMN, complex I assembly is disrupted, and the individual subunits of complex I undergo degradation.

2. Materials and methods

Animals. All animal procedures conformed to the EU Directive 86/609/EEC and Recommendation 2007/526/EC regarding the protection of animals used for experimental and other scientific purposes, enforced by Spanish law under Real Decreto 53/2013. The mice were housed in pathogen-free animal facility at CNIC, Madrid with an artificial 12 h light cycle; temperature was kept at 22 °C ± 2, relative humidity oscillated between 45 % and 65 %. Mice were fed standard chow diet (LASQCdiet® and from December 2021 D184 SAFE®).

Cell lines: all cell lines were grown in complete DMEM medium (D5796, containing 4500 mg/L glucose, 2 mM L-glutamine) supplemented with 10 % fetal bovine serum (FBS, Sigma F7524), 1 % penicillin-streptomycin (PenStrep, Lonza) and 1 mM sodium pyruvate (Pyr, Sigma), at 37 °C in an atmosphere of 5 % CO_2/95 % air (Table 1). Mouse adult fibroblasts (MAFs) were isolated from mouse ear of at least 2 different female mice: mouse ears were cut, incubated with collagenase (1 %, 10 min at 37 °C) and seeded in 24-well plates with the same medium as stated before, supplemented with 1 μg/ml Amphotericin B. After the first three passages, cells were immortalized with a lentiviral vector expressing the SV40 large T antigen (pLOX-Ttag-iresTK, Addgene).

Estimation of cellular proliferation: For growth curves the CYQUANT™ NF Cell Proliferation Assay Kit (ThemoFisher Scientific C35006) was used following manufacturer instructions. Cells were grown in DMEM medium supplemented with 5 % dialyzed FBS, 1 mM Pyr and either glucose 5 mM or galactose 5 mM. 2000 cells were seeded in 96-well plates and were grown for 3 days. Each day, fresh medium with or without inhibitors were added. Cell number was estimated by fluorescence (Excitation: 488 nm; Emission: 535 nm) after incubation with CYQUANT™ 30 min at 37 °C in the dark. Cell proliferation was calculated as the ratio between (estimated) number of cells at day 72 h and at the moment of the beginning of the experiment.

Riboflavin free medium: Riboflavin free medium was prepared from RPMI 1640 Medium w/o L-Alanine, L-Glutamine, Folic acid, Riboflavin Culture Media powder (MyBioSource). Following manufacturer instructions. Briefly, 10.092 g of powder were dissolved in 900 ml of ddH_2O_2 by 3 h stirring at room temperature. Then, 2 mM L-glutamine, 10 % dialyzed fetal bovine serum (Sigma), 1 % penicillin-streptomycin (Sigma), 1 mM sodium pyruvate (Sigma), 8 mg L-Alanine (sigma), 2 mg Folate (Sigma) were added, the pH was adjusted to 7.1 with HCl, the volume was adjusted to 1 L with ddH_2O_2 and the mix was kept stirring for additional 30 min at room temperature. After that, pH was re-checked and 2 g of sodium bicarbonate were added and stirring was kept for additional 5 min. Control cells were grown in the same media with the addition of 1 μM riboflavin. Without riboflavin, cell proliferation decreased gradually and stopped after ten days; after five days, passaging cells already become difficult. For these reasons, it was important to plate a sufficient number of cells before the withdrawal of the vitamin.

Table 1
Cell lines used in this study.

Cell line	Comments
FC57 MAFs	L929 nuclear background and C57BL/6 mtDNA [21]
143B	Human osteosarcoma cell line [22]
Clpp −/− MAFs	Gift from Alexandra Trifunovic lab [23]
Ndufs4 −/− MAFs	Generated in this study
143B *SLC25A32*^{KO}	Generated in this study

Mitochondria isolation and functional assays. Isolation of mitochondria from cell cultures was performed from 4 to 10 150 mm plates, according to the differential centrifugation method. Briefly, cells were lysed by hypotonic shock with 7 vol of hypotonic medium (83 mM sucrose, 10 mM MOPS, pH 7.2) and homogenized in a Teflon potter-type tissue homogenizer. Then, 7 vol of hypertonic medium (sucrose 510 mM, MOPS 30 mM, pH 7.2) were added. The homogenate was centrifuged at 1000 g, 5 min, the supernatant obtained was centrifuged at 10,000 g, 10 min. The pellet obtained was resuspended in medium A (0.32 M sucrose, 1 mM EDTA, 10 mM Tris-HCl, pH 7.4) and stored at −80 °C. Isolation from mouse kidney was similar, medium A was used throughout all homogenization steps. In case mitochondria were used fresh for functional assays (ex. respirometry), medium A supplemented with bovine serum albumin 0.1 % was used throughout all homogenization steps.

Spectrophotometric activities. Enzyme activities were calculated according to the Beer-Lambert law by kinetic analysis of the absorbance variation measured by a UV–visible spectrophotometer. All assays were performed at 32 °C in 1 ml cuvettes, using frozen-thawed mitochondria resuspended in activity buffers. Complex I activity was initiated by addition of 130 μM NADH and monitored at 340 nm (ε = 6.22 $mM^{-1}cm^{-1}$). Rotenone-insensitive rates were measured in parallel and subtracted from the measured rates. For NADH:O_2 activity, 10 μg of mitochondria were resuspended in sucrose buffer (250 mM, HEPES 2 mM, EGTA 0.1 mM) and pre-incubated for 10 min with the inhibitor or DMSO plus 130 μM NADH. For NADH:decylubiquinone activity 10 μg of mitochondria were resuspended in sucrose buffer plus 1 μg/ml antimycin A and 130 μM decylubiquinone. For complex II activity, 30 μg of mitochondria were resuspended in sucrose buffer plus 100 μM dichlorophenol-indophenol (DCPIP), 1 μg/ml antimycin A, 130 μM decylubiquinone and 1 μM rotenone. The reaction was initiated by addition of 10 mM succinate and monitored at 600 nm (ε = 19.2 $mM^{-1}cm^{-1}$). For citrate synthase activity, 5 μg of mitochondria were resuspended in 10 mM Tris-HCl pH 8, 0,1 % Triton X-100, 46 μg/ml acetyl-CoA, 200 μM 5,5-Dithio-bis-2-nitrobenzoic acid (DTNB). The reaction was initiated by addition of 0.5 mM oxaloacetate and monitored at 412 nm (ε = 13.6 $mM^{-1}cm^{-1}$).

Respirometry. Oxygen consumption was assayed using a Clark type polarographic oxygen sensor (Oroboros instruments) in a 2 ml isolated chamber, in agitation with a magnetic stirrer, at 37 °C, in Mir 05 respiration medium (Oroboros instruments). Either 50 μg of mitochondria or 2 million of cells permeabilized with 20 μg of digitonin were sequentially incubated with the indicated substrates and inhibitors. Respiration following antimycin A incubation was set as baseline; complex IV respiration was calculated as ascorbate/TMPD minus azide oxygen consumption rate.

Flavin fluorescence assay. Flavin fluorescence in mitochondria and in cells was measured following the protocol of [24]. Briefly, either 2 million of cells or 50 μg of mitochondria were resuspended in Tris-HCl 10 mM pH = 7.5 and incubated on ice for 10 min to allow lysis by osmotic shock. Flavin fluorescence was measured at 435/550 nm (em/ex) in a plate fluorescence reader. A regression line was built in parallel using known concentration of FAD. The flavin independent background fluorescence was subtracted by adding in each well a reducing solution of sodium dithionite, because reduced flavin have no fluorescent emission. Flavin fluorescence in CN gels were revealed with an iBright scan (Invitrogen) after 2 min incubation of the gel in a solution with 2 % SDS, 1 % β-mercaptoethanol. During the preparation of this manuscript a similar protocol was published elsewhere [25].

Quantitative analysis of flavins. Mitochondrial and cytosolic samples purified from cells DPI-treated and untreated were boiled for 5 min, and then precipitated proteins and cellular remains were removed by centrifugation. Supernatant was then analyzed using an Alliance HPLC system (Waters) equipped with a 2707 autosampler and a HSST3 column (4.6 × 50 mm, 3.5 mm; Waters) preceded by a pre-column of the same material (4.6 × 20 mm, 3.5 mm; Waters). An aliquot of 50 μl of the

solution was applied and the chromatography was developed at 1 ml/min with a 6 min isocratic run of methanol 40 % (vol/vol) in 5 mM ammonium acetate pH 6.0 [26]. RF, FMN and FAD standard curves acquired under the same conditions were used to quantify the flavin content present at each assayed condition.

Mitochondria solubilization. Solubilization of mitochondrial membranes was carried out with digitonin, in order to visualize both respiratory SCs and free form complexes. The ratio of grams of detergent: grams of mitochondrial protein used was 4:1.100 μg of purified mitochondria were incubated with digitonin for 5 min in 50 mM NaCl buffer, 50 mM imidazole, 5 mM aminocaproic acid at a concentration of 10 μg/μl. The insoluble fraction was removed by centrifugation at 13,000*g* in microfuge for 30 min at 4 °C. The pellet obtained was discarded and the supernatant was mixed with 4× loading buffer (5 % Coomassie Blue-G**25**0 in 1 M aminocaproic acid) for gel loading.

Preparation of polyacrylamide gels. Gradient polyacrylamide gels were prepared in house with a gradient former, composed of two chambers, where two solutions of different percentage of acrylamide were added. Mini Protean III system (Biorad) 1.5 mm was used normally, for mass spectrometry experiments, larger gels (23 × 16.5 cm) were used. The gradient used was different depending on the kind of high molecular weight SCs that wanted to be visualized, in general, for the resolution of SCs and complexes (DIG) gels were 5–13 % [27]. CN gels were essentially the same, but 0.01 % of digitonin was added to all gel solutions and Ponceau red buffer (Ponceau red, glycerol) was used instead of the normal loading buffer.

BN-PAGE and CN-PAGE. The amount of sample loaded in each well was that obtained from solubilization of 100 μg of mitochondria, except in the case of samples intended for analysis by mass spectrometry, for which samples were of 300 μg. Cathode buffer A (tricine 50 mM, bis-tris 15 mM, pH 7.0, Coomassie Blue G-250 0.02 %), cathode buffer B (tricine 50 mM, bis-tris 15 mM, pH 7.0, Coomassie Blue G-250 0.002 %) and anode buffer (bis-tris 50 mM, pH 7.0) were used for electrophoresis. Electrophoresis was performed in cold chamber. The run was developed for half hour at 90 V with cathode buffer A. Then, the cathode buffer was exchanged for cathode buffer B and electrophoresis continued for approximately one more hour at 300 V. In CN gels the whole electrophoresis was performed in cathode buffer B, with no changes. From the electrophoresis it was possible to reveal the activity of respiratory complexes in gel, to perform western blotting with antibodies against proteins of the respiratory complexes, to stain the gel to later analyze the gel composition by mass spectrometry, or reveal flavin fluorescence.

SDS-PAGE. Electrophoresis for protein separation was performed in denaturing polyacrylamide gels. The protein samples were incubated for 1 min at 95 °C with loading buffer (Tris-HCl 50 mM pH 6.8, 2 % SDS, 10 % glycerol, 1 % β-mercaptoethanol, 0.02 % bromophenol blue). Subsequently, 30 μg of each protein sample was loaded on a 12.5 % acrylamide gel and electrophoresis was developed in Tris-glycine solution at 10 mA per gel during migration on the stacking gel and at 20 mA per gel once the sample passed to the resolving gel.

Immunoblotting. Immunodetection by Western blot was performed on either type of electrophoresis previously described. Briefly, proteins were transferred to PVDF membrane (Immobilon-FL, 0.45 μm) by transfer in Bio Rad Mini *Trans*-Blot Cell or *Trans*-Blot Cell systems, in 48 mM Tris, 39 mM glycine, 20 % methanol transfer solution, 1 h at 100 V or o/n at 30 V. Once the membrane was obtained, it was blocked in 0.1 % PBS-tween, 5 % BSA solution for 1 h and incubated with primary antibody overnight in agitation at 4 °C (Table 2). After three washes with 0.1 % PBS-tween, it was incubated with secondary antibody for 1 h, after which another three washes were performed before development. Membrane revealing was performed by using fluorescent secondary antibody and revealed with the Odyssey imaging system (LI-COR biosciences).

Complex I In-gel activity. Measurement of NADH dehydrogenase activity of complex I was determined on the same gel after BN-PAGE electrophoresis. The gel was incubated in 0.1 M Tris-HCl, pH 7.4, 0.14 mM NADH and 1 mg/ml NitroBlue tetrazolium solution at room temperature. Visualization was achieved by the purple precipitate produced after reduction of NitroBlue tetrazolium by the NADH dehydrogenase activity of CI.

Table 2
Antibodies used in this study.

Target	Origin/conjugate	Clonality	Company
ACAD9	Mouse	Poli-	Abcam
Actin	Rabbit	Poli-	Sigma
CS	Rabbit	Mono-	Abcam
COX1	Mouse	Mono-	Invitrogen
NDUFA9	Mouse	Mono-	Abcam
NDUFS1	Rabbit	Poli-	Abcam
NDUFS2	Rabbit	Poli-	Abcam
NDUFS3	Mouse	Mono-	Abcam
NDUFS4	Mouse	Mono-	Abcam
NDUFS5	Rabbit	Poli-	Proteintech
NDUFV1	Rabbit	Mono-	Sigma
NDUFV2	Rabbit	Mono-	Abcam
SDHA	Mouse	Mono-	ThermoFisher
TOM20	Rb	Poli-	Santa Cruz
UQCRC2	Mouse	Mono-	Abcam
UQCRFS1	Mouse	Mono-	Abcam
VDAC	Mouse	Mono-	Abcam
Anti-Mouse	DyLight 800™	Poli-	Rockland
Anti-Rabbit	DyLight 800™	Poli-	Rockland
Anti-Mouse	AlexaFluor 680	Poli-	LIfe technologies
Anti-Rabbit	AlexaFluor 680	Poli-	LIfe technologies

CRISPR/Cas9 genome editing. KO cell lines were generated by CRISPR/Cas9 mediated genome editing with the TLCV2 viral vector (Addgene) [28]. A two-target sequence strategy was employed. Target sequences were generated using the CHOP/CHOP tool [29]. The two-best gRNA, in terms of low off-target and high on-target activity, were chosen against the first exon of the *SLC25A32* gene (Table 3). The sequences were cloned in two TLCV2 vectors and used to transduce cells. A non-targeting gRNA was used to generate a control cell line. Lentivirus production was carried out by the Viral Vector unit at CNIC. After two days of transduction, puromycin 1 μg/ml was added to select transduced cells. After one day of selection doxycycline was added to induce the expression of Cas9. The following day GFP positive cells were seeded in a 96 wells plate containing conditioned DMEM of the parental line, one cell per well. For the following weeks the growth of clones was monitored. Clone screening was performed by PCR, using primers flanking the PAM sequences targeted by the two sgRNAs. The clones which presented abnormal PCR amplicons were grown. Since no good anti SLC25A32 antibody was found, the knockouts were validated by qPCR.

Proteomics analysis. High-Throughput protein profiling was performed in collaboration with the CNIC-proteomics Unit. Total cellular pellet of 143 B cells was digested with trypsin and labelled with tandem mass tags TMT (10 plex), according to manufacturer's instructions. Resulting tryptic peptides were injected onto a C-18 reversed phase (RP) nano-column (75 μm I.D. and 50 cm, Acclaim PepMap, Thermo Fisher, San José, CA, USA), connected to a nEasy LC-1000 chromatography system (Thermo Fisher, San José, CA, USA) and analyzed in a continuous acetonitrile gradient consisting of 8–31 % B-solution (B = 0.5 % formic acid in acetonitrile) for 240 min, 50–90 % B for 1 min. Subsequently, peptides were eluted from the RP nanocolumn at a flow rate of ~200 nL/

Table 3
Primers used in this study.

Name	Primer
hSLC25A32_g1 *Bsb*I Fwd	CACCGAATAGGGGTCGCAAGCACGGGGG
hSLC25A32_g1 *Bsb*I Rev	AAACCCCCCGTGCTTGCGACCCCTATTC
hSLC25A32_g2 *Bsb*I Fwd	CACCGTGGGAACACGTTTATTCCAGAGG
hSLC25A32_g2 *Bsb*I Rev	AAACCCTCTGGAATAAACGTGTTCCCAC
hSLC25A32_ex1 Fwd	GCATAAGAGTCCTCTCGTTGGT
hSLC25A32_ex1 Rev	AAAAGACGGAGGAGATCCAGTT

min to an emitter nanospray needle for real-time ionization and MS analysis in a Q-Exactive HF mass spectrometer (Thermo Fisher). Mass spectra were acquired in a data-dependent manner, with an automatic switch between MS and MS/MS using a top 20 method. The raw files were analyzed with Proteome Discoverer (version 2.1, Thermo Fisher Scientific), using Uniprot database. The parameters selected for database searching were: trypsin digestion with 2 maximum missed cleavage sites, precursor mass tolerance of 800 ppm, fragment mass tolerance of 0.03 atomic mass unit (amu). MS/MS spectra were also queried against inverted databases constructed from the same target databases. Peptide identification from MS/MS data was performed using the probability ratio method [30]. False discovery rates (FDR) of 1 % was used as a threshold for peptide identification. Quantitative information were extracted from TMT reporters ions in the MS/MS spectra, and protein abundance changes were analyzed using the WSPP model [31] by applying the Generic Integration Algorithm [32].

Transcriptomic analysis. RNA sequencing was performed by the team of CNIC Genomics Unit. Downstream analysis was performed by CNIC Bioinformatics Unit. RNA libraries were produced using TrueSeq RNA-Seq kit from Illumina and sequenced in the HiSeq 2500 Illumina Sequencer. Adaptors from RNAseq were removed from reads using the trimgalore v-0.6.6 and cutadapt v-1.18 software. Then, trimmed reads were mapped and quantified on the transcriptome GRCm38 gene-build 91 using RSEM v-1.3.1 [33]. Data were then normalized by using trimmed mean of M-values method [34] and differential expression analyzed using the function Voom from the bioconductor package Limma v-3.50.3 [35]. False discovery rate was corrected using Benjamini–Hochberg method, considering differentially expressed genes for an adjusted p-value ≤0.05. Pathway enrichment analysis was performed GSEA software [36,37] through REACTOME pathways database [38]

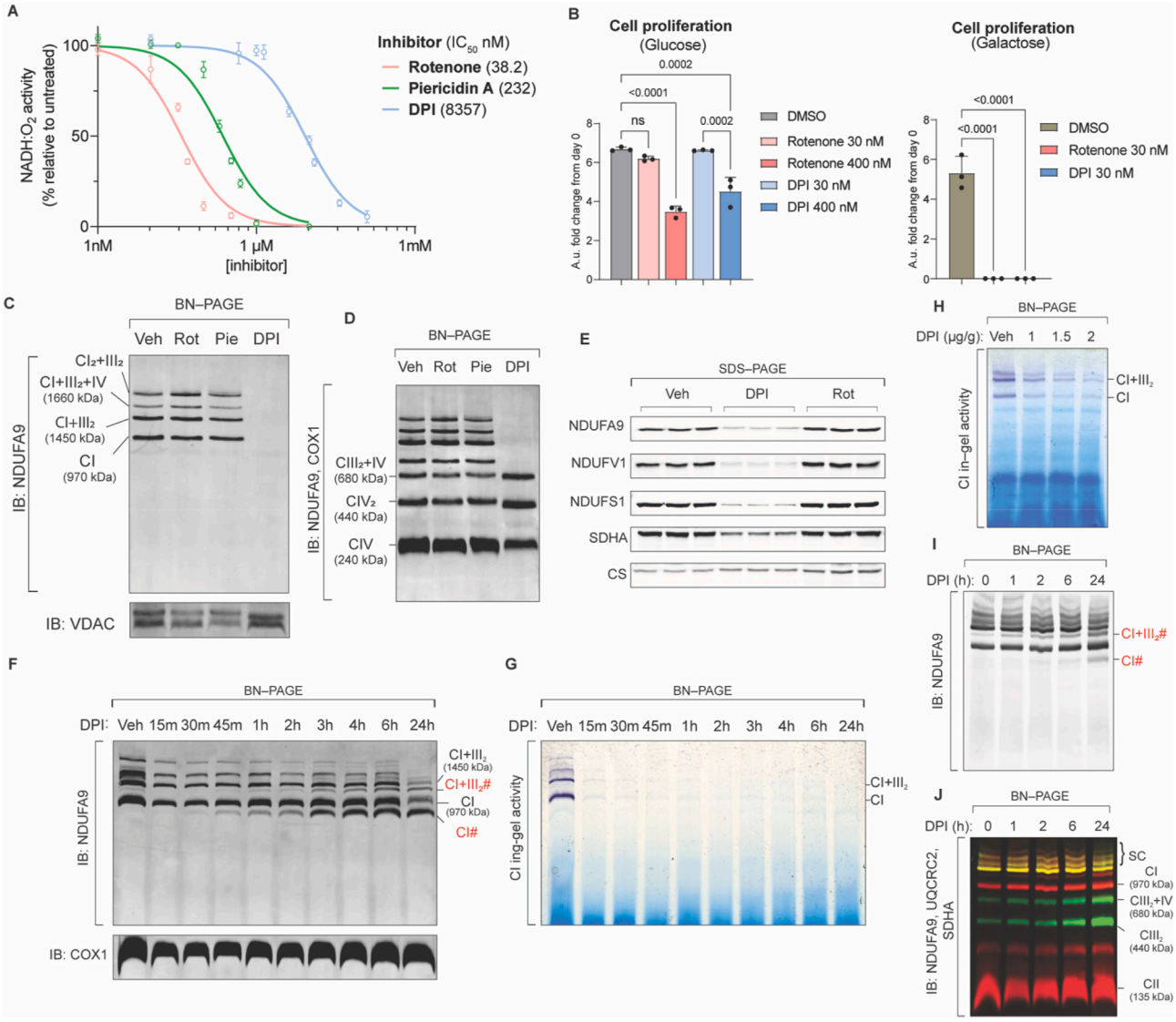

Fig. 1. Diphenyleneiodonium induces respiratory complex I degradation. (A) Inhibition of complex I NADH:O_2 activity of frozen-thawed mouse kidney mitochondria by rotenone, piericidin A and DPI. Samples were pre-incubated for 10′ in the presence of NADH and the indicated inhibitor, n = 3 replicates per point. **(B)** Effect of 72 h DPI and rotenone treatment on MAFs cell proliferation in glucose or galactose media. Data are mean ± S.E.M., ordinary two-way ANOVA, Dunnett's multiple comparisons test. **(C, D)** Immunoblot analysis of the effect of 72 h, 1 µM DPI, rotenone or piericidin A treatment on the supramolecular organization of complex I (C), complex III and complex IV (D), Veh = DMSO. **(E)** Immunoblot analysis of the effect of 72 h, 400 nM DPI and rotenone on complex I and complex II subunits abundance relative to citrate synthase. The quantification is displayed in Fig. S1A. **(F)** Immunoblot analysis of the short-term effect of 400 nM DPI treatment on the supramolecular organization of complex I. "CI#" and "CI + III_2#" refer to complex I and supercomplex CI + III_2 sub-complex, respectively. **(G)** In-gel activity analysis of the short-term effect of DPI on complex I. **(H–J)** In-gel activity (H) and immunoblot analysis (I and J) of the effect of 2 µg/g DPI *i. p.* Injection on kidney mitochondria complex I.

using log_2FC values as the gene ranks. Transcription factor activity was inferred by virtual inference of protein activity by enriched regulon analysis (VIPER) [39] using DoRothEA regulons [40]. We filter for regulons with level of confidence ("A" and "B") and we filtered out genes with an adjusted p value of the log_2FC greater than 0.0001. Generation of heatmaps and Figures was done in R using Complex Heatmap package [41].

3. Results

3.1. Diphenyleneiodonium induces respiratory complex I degradation

In isolated mitochondria, the NADH:ubiquinone oxidoreductase activity of respiratory complex I is sensitive to the *N*-site inhibitor diphenyleneiodonium (DPI) [20]. Compared with piericidin A and rotenone, two commonly used Q-site inhibitors, DPI is at least one hundred times less potent (Fig. 1A) [42]. However, DPI treatment completely suppresses cell division of immortalized mouse adult fibroblasts (MAFs) in galactose medium, showing that it interferes with cellular respiration as rotenone does (Fig. 1B). We have previously demonstrated that deficiency of complex III leads to the degradation of complex I, and that the use of rotenone effectively inhibits this degradation process [43]. In this study, we aimed to investigate whether the site of complex I inhibition has any effect on the structural organization of complex I within the mitochondrial electron transport chain.

To explore this, we conducted experiments using mitochondria isolated from MAFs cultivated in glucose medium and treated with different complex I inhibitors (DPI, rotenone, and piericidin) for a duration of 72 h. Isolated mitochondria were then solubilized with digitonin and analyzed by blue-native gel electrophoresis (BN-page). Surprisingly, we observed that treatment with DPI resulted in a complete and selective loss of respiratory complex I and its associated supercomplexes, I + III_2 and I + III_2+IV (Fig. 1C), with no effect on other respiratory complexes (Fig. 1D). In contrast, the Q-site inhibitors rotenone and piericidin A did not exhibit any noticeable changes in the BN-page profile of the mitochondria. To further validate these findings, we performed a similar experiment but employed denaturing conditions using SDS-page. Consistent with our previous results, MAFs treated with DPI showed a decrease in the abundance of complex I subunits, whereas rotenone treatment did not (Fig. 1E and Fig. S1A). This result highlights a unique feature of the *N*-site inhibitor DPI, which piqued our interest and prompted us to investigate deeper its mechanism of action.

In subsequent experiments, we observed a correlation between the loss of complex I and the appearance of faster migrating bands below complex I and complex I-containing supercomplexes on the BN gel (marked as "CI#" and "CI + $CIII_2$#", Fig. 1F). The accumulation of the "sub-complexes" was time-and dose-dependent: it started after 45 min, it peaked after 4–6 h, and by 72 h all holo- and sub-complexes had disappeared (Fig. 1F, Fig. S1, B and C; for 72 h see Fig. 1, C and F). On the other hand, inhibition of in-gel NADH:NBT oxidoreductase activity occurred immediately without any lag time (Fig. 1G).

To validate the impact of DPI on complex I beyond cell culture, we administered DPI intraperitoneally (*i.p.*) to wild-type CD1 mice. DPI treatment resulted in the inhibition of complex I and the accumulation of complex I sub-complexes *in vivo*, as evidenced by Fig. 1H and I. At the 24-h time point, the abundance of $CIII_2$ and $CIII_2$–CIV complexes appeared to increase, likely due to their detachment from complex I-containing supercomplexes subsequent to DPI treatment (Fig. 1J).

3.2. Molecular characterization of complex I "sub-complexes"

To gain insights into the nature of the observed "sub-complexes," we employed two complementary approaches. Firstly, we resolved respiratory complexes by two-dimensional BN/SDS-page. Subsequent immunoblot analysis showed the absence of NDUFS1, NDUFV1, NDUFV2 and NDUFS4 subunits from the bands corresponding to the "sub-complexes" (Fig. 2A and B). These subunits belong to the *N*-module, which is the NADH-oxidizing region of complex I where the FMN cofactor binds. Importantly, DPI acts specifically at this site. We further confirmed the absence of the *N*-module from all subcomplexes by simultaneous incubation with antibodies against *N*-module subunit NDUFS1 and Q-module subunit NDUFA9 in one-dimensional BN gels (Fig. 2C).

Secondly, we analyzed by LC-MS the proteins present in the BN-gel bands corresponding to holo-complex I and sub-complex I. The results revealed that all subunits of the *N*-module were absent from the sub-complex (Fig. 2D), in agreement with the findings of the BN/SDS two-dimensional page experiment. Our proteomic analysis also identified several complex I assembly factors co-migrating with the sub-complex (Fig. 2D). The overall composition of this sub-complex corresponds to the 830 kDa "Q/P″ assembly intermediate previously described in Ref. [12]. This assembly intermediate represents the final step in the complex I assembly pathway before the placement of the *N*-module. Accordingly, we observed the accumulation of NDUFAF2, a factor that specifically binds to the Q/P assembly intermediate, upon DPI treatment (Fig. 2E).

Our findings indicate that DPI treatment induces the loss of complex I in a bimodal pattern. Initially, the subunits of the *N*-module (including NDUFS1, NDUFV1, NDUFV2, and NDUFS4) are lost and the Q/P assembly intermediate accumulates. Subsequently, the subunits belonging to the Q- and *P*-modules start to be degraded as well, leading to the complete loss of the entire complex I (Fig. 2F–H). In these blots, we noticed also the reduction of the SDHA subunit of complex II; the reasons behind this phenomenon will be clarified later.

3.2.1. DPI blocks complex I assembly

The fact that Q/P assembly intermediates accumulate in cells and animals treated with DPI can be explained by two, not-mutually exclusive, hypotheses: (i) DPI interferes with the maturation of the *N*-module, leading to its destabilization and preventing its proper insertion into the holo-enzyme. Consequently, complex I assembly cannot be completed and Q/P intermediates accumulate; (ii) DPI causes the degradation of the *N*-module once it's already on complex I. The Q/P intermediate is the product of this degradation which, therefore, accumulate.

To distinguish between these two, we conducted experiments using freshly isolated mitochondria, which lack the input of nuclear-encoded subunits from the cytosol, and thus display minimal CI assembly. In this *in vitro* experiment, the Q/P assembly intermediate did not accumulate despite the complete inhibition of complex I by DPI (Fig. 3A), and we could only observe the accumulation of relevant but minute amounts of "CI + $CIII_2$ sub-complex" (marked as CI + $CIII_2$#, Fig. 3A, bottom blot). This observation was consistent even when mitochondria were maintained in a coupled respiring state for up to 8 h at 37 °C. These results suggest that the accumulation of Q/P complexes is mostly due to stalled complex I assembly.

We then utilized a mitochondrial translation inhibitor, chloramphenicol (CAP), to further validate this point. CAP selectively disrupts the assembly of respiratory complexes I, III, IV, and ATP synthase, as they require the synthesis of mtDNA-encoded peptides. Once CAP is removed from cell medium, mitochondrial translation resumes, enabling gradual rebuilding of oxidative phosphorylation complexes [12]. In our experiment, we treated MAFs with CAP for 5 days, completely depleting them of complex I. Subsequently, we washed out CAP and provided fresh medium containing either DMSO (control) or DPI (Fig. 3B). In the control group treated with DMSO, complex I was fully reassembled within 24 h, as expected. In contrast, cells treated with DPI were able to assembly only Q/P intermediates (Fig. 3C). Next, we conducted a complementary experiment by treating cells with DPI and CAP simultaneously. In this setup, we adjusted the duration of CAP treatment to two days in order to preserve the already existing complex I, while blocking the assembly of new complexes (Fig. 3D). Under these conditions, the presence of CAP prevented the accumulation of Q/P

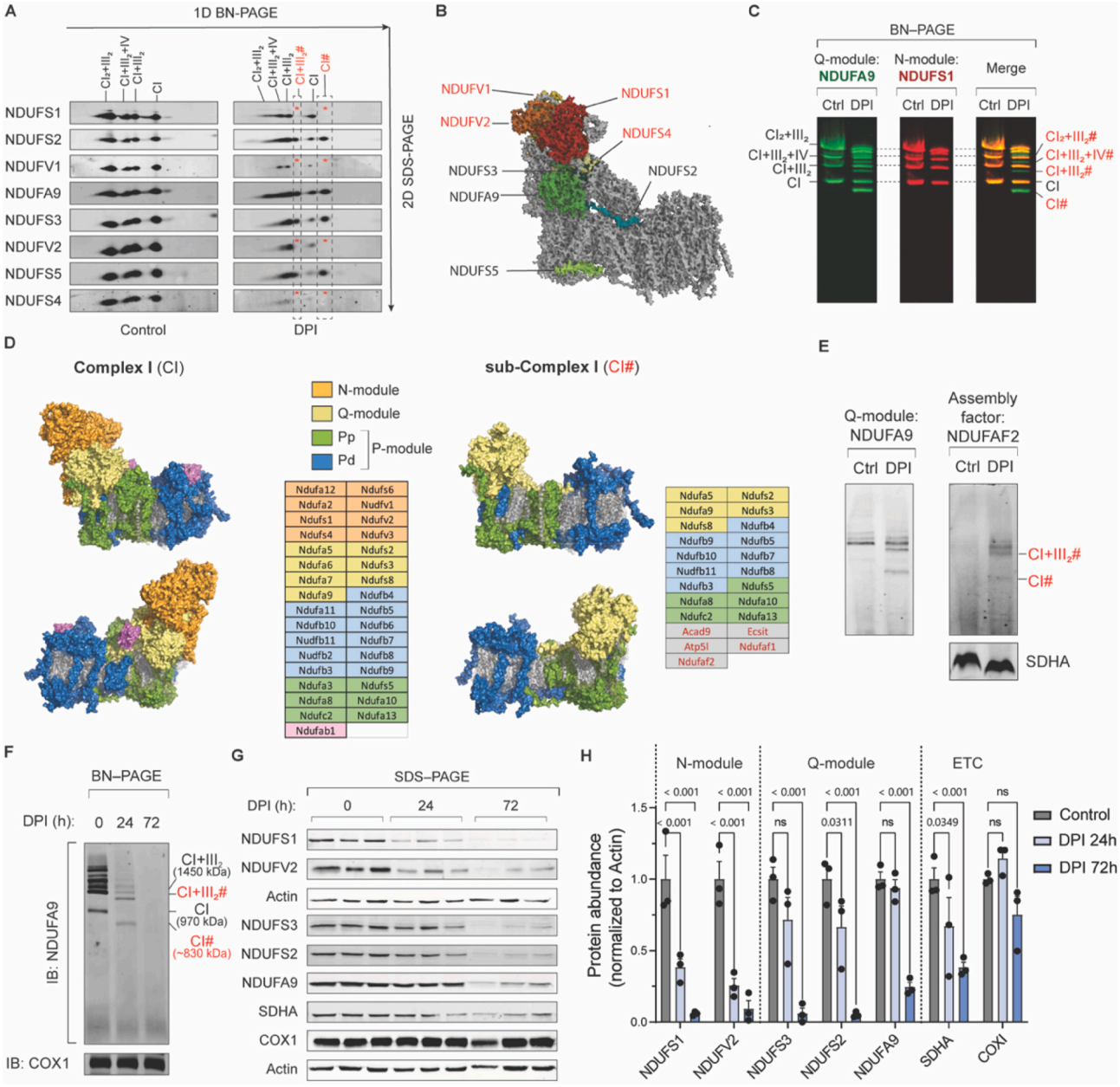

Fig. 2. Molecular characterization of complex I sub-complexes. (A–B) Subunit composition of complex I sub-complexes revealed by immunoblot analysis of two-dimensional BN/SDS polyacrylamide gel (A) and localization of the subunits in the structure of complex I (B), (PDB accession number: 5LDW, *N*-module subunits are in red). In (A), MAFs were treated with 400 nM DPI for 24 h. **(C)** Immunoblot analysis of the subunit composition of complex I sub-complexes revealed by co-incubation of *N*-module and Q-module specific antibodies. Mitochondria isolated from MAFs treated with 400 nM DPI for 24 h. **(D)** Structural complex I models summarizing the results from LCMS analysis of in-gel digested BN-PAGE CI and CI# bands. The two eluted bands are the same as CI and CI# bands from Fig. 2C. The color code for the modules was adopted from Ref. [12]. Pink, NDUFAB1; shady gray, subunit not found in either band. **(E)** Immunoblot analysis of the accumulation of NDUFAF2 assembly factor upon DPI treatment. Mitochondria isolated from MAFs treated with 400 nM DPI for 24 h **(F)** Comparison between the short-term and long-term effect of 400 nM DPI treatment on complex I. **(G–H)** Immunoblot analysis of the effect of short-term and long-term 400 nM DPI treatment on *N*-module and Q-module subunits abundance (G) and quantification relative to β-actin (H). Data represented as mean ± S.E.M, ordinary two-way ANOVA, Dunnett's multiple comparisons test. (For interpretation of the references to color in this figure legend, the reader is referred to the Web version of this article.)

intermediates upon DPI treatment (Fig. 3E).

The findings from the combined DPI and CAP treatment experiments, along with the previous observations, collectively indicate that the nature of the subcomplexes is that of a stalled assembly intermediate with a minor contribution resulting from holo-complex degradation.

3.2.2. *Acute DPI treatment results in N-module degradation*

These results suggest that the last step of complex I assembly can be disrupted by DPI treatment *in vivo*. DPI is known to form covalent adducts with flavin cofactors [44] and with complex I FMN [20]. We hypothesized that DPI could react with the FMN cofactor as soon as it is inserted into the nascent *N*-module assembly intermediate, destabilizing it (Fig. 4A). Since free *N*-modules are not typically accumulated in wild-type cells, we utilized the *Ndufs4*$^{-/-}$ model in which a significant proportion of the *N*-module is dislodged from the enzyme and can be visualized as a separate band in the lower part of the BN gel [45]. In *Ndufs4*$^{-/-}$ MAFs, DPI led to a rapid loss of the *N*-module (Fig. 4B). In isolated mitochondria from *Ndufs4*$^{-/-}$ animals, *in vitro* DPI treatment

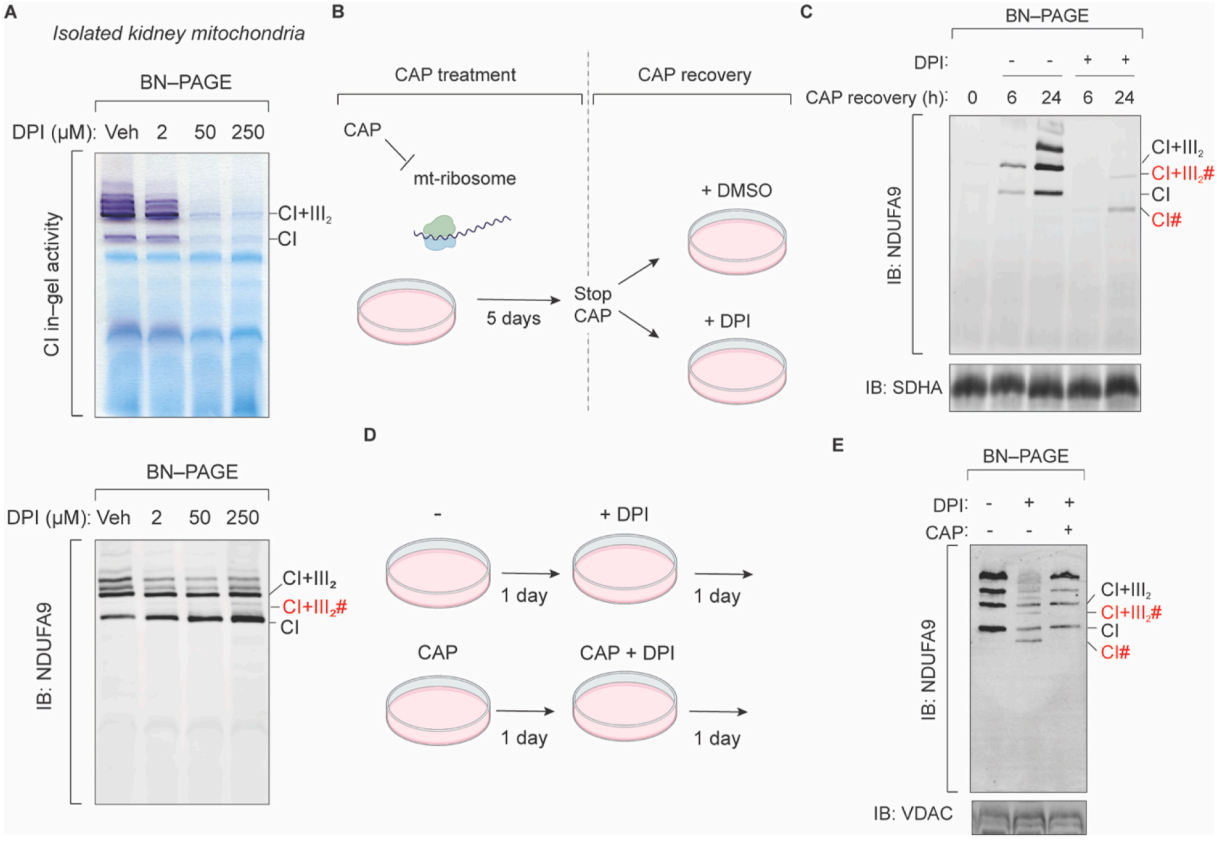

Fig. 3. DPI blocks complex I assembly by destabilization of the *N*-module. (A) In-gel activity analysis (top) and immunoblot (bottom) of mitochondria isolated from mouse kidney and then treated *in vitro* with DPI for 4 h at 37 °C. Note that, when DPI is added after the isolation of mitochondria, complex I is not destabilized, in spite of the complete inhibition of its activity at DPI>50 μM; Veh = DMSO. **(B, C)** Experimental scheme (B) and immunoblot analysis (C) of the effect of 50 nM DPI treatment on CAP pre-treated MAFs. **(D, E)** Experimental scheme (D) and immunoblot analysis (E) of the effect of 50 nM DPI treatment on CAP co-treated MAFs. All experiments are representative of at least 2 replicates.

inhibited the in-gel activity of both the *N*-module and the holo-complex I, but specifically caused the loss of the *N*-module with minor effect, if any, on the assembled complex I (Fig. 4C and D). Therefore, DPI inhibits the reaction between NADH and FMN of both complex I and the isolated *N*-module, but destabilizes only the *N*-module when it is not inserted in complex I.

To gain further insight into the impact of FMN loss on the stability of the *N*-module, we employed computational models to investigate the energy changes occurring within the interacting subunits of the *N*-module (Fig. 4E). Our computational analysis validated that the absence of FMN results in destabilization, as evidenced by an increase in free energy, of the interactions between the *N*-module subunits NDUFV1, NDUFV2, and NDUFS1. These pairwise energy differences, influenced by the presence or absence of FMN, suggest that the absence of FMN induces an overall rearrangement of side chains within the *N*-module. This rearrangement subsequently triggers a cascade of changes, akin to a generalized butterfly effect, ultimately resulting in a decrease in *N*-module cohesion.

Following the depletion of FMN by DPI, the *N*-module subunits become dissociated and undergo rapid degradation. Previous studies have identified several *N*-module subunits as substrates of ClpPX, an ATP-dependent mitochondrial protease [23]. To investigate the role of ClpPX in the degradation process induced by DPI, we examined the effect of DPI treatment in cells lacking CLPP, a key component of ClpPX. In *Clpp*$^{-/-}$ cells, DPI treatment resulted in the rapid loss of complex I and the most prominent *N*-module band (Fig. 4F). Concurrently, we observed the accumulation of the free NDUFS1 subunit in the lower region of the gel (Fig. 4F). These findings agree with the proposal that ClpXP plays a crucial role in the degradation of *N*-module subunits upon their release from complex I triggered by DPI [23].

3.2.3. *DPI treatment activates the integrated stress response and inhibits cholesterol biosynthesis*

Having elucidated the nature and accumulation of the Q/P subcomplex, our investigation shifted towards understanding the long-term consequences of DPI treatment, specifically the complete loss of complex I. In patients harboring mutations in nuclear genes responsible for encoding *N*-module subunits, the same Q/P subcomplex accumulates, but it is not subjected to degradation[46,47]. This observation led us to hypothesize that the degradation of the entire complex I following DPI treatment might be attributed to an additional effect of DPI rather than the accumulation of the Q/P subcomplex alone.

To gain a comprehensive understanding of the global impact of DPI treatment on MAFs, we conducted RNA-seq analysis at 24- and 72-h following treatment. Interestingly, the gene expression profiles at these two time points exhibited significant overlap. However, it is worth noting that at the 72-h time point, gene expression tended to revert towards control levels. At the 24-h time point, we identified 459 downregulated and 315 upregulated high-confidence genes (adjusted p-value >0.001, Supplementary Data 1). The transcripts of complex I genes showed minimal changes, implying that the observed loss of complex I subunits primarily occurs through post-transcriptional mechanisms. This finding aligns with previous studies suggesting that the regulation of complex I levels primarily occurs at the protein level rather than at the transcriptional level [48].

To gain further insights into the functional implications of DPI treatment, we performed gene set enrichment analysis (GSEA) [36,37] utilizing $\log_2$FC values as gene ranks (Fig. 5A). The analysis of

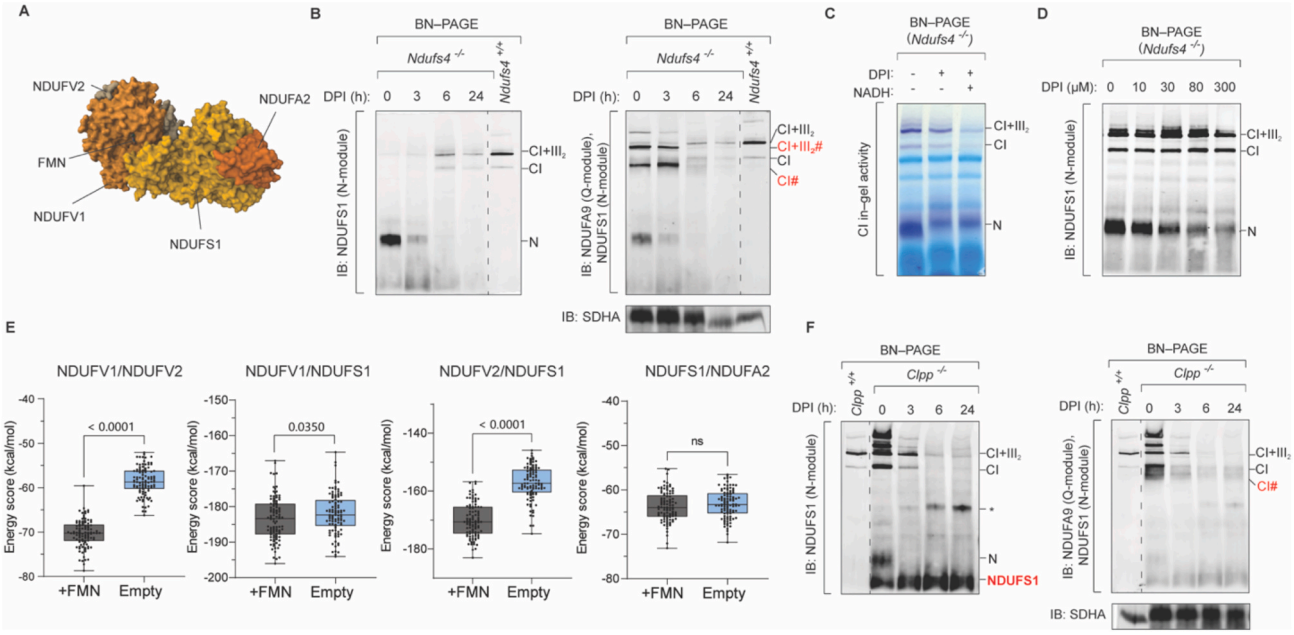

Fig. 4. DPI destabilizes isolated complex I *N*-module. (A) Schematic representation of complex I *N*-module (PDB accession number: 6G2J). **(B)** Immunoblot analysis of the effect of 50 nM DPI treatment on *Ndufs4*$^{-/-}$ MAFs, revealed using antibodies against the *N*-module (left) or against both the *N*- and the Q-module (right). **(C)** In-gel activity of mitochondria isolated from *Ndufs4*$^{-/-}$ mice and then treated with 300 μM DPI. 300 μM NADH was added to reduce complex I FMN, allowing its reaction with DPI. **(D)** Immunoblot analysis of mitochondria isolated from *Ndufs4*$^{-/-}$ mice and then treated with DPI for 4 h at 37 °C, revealed with an antibody against the *N*-module. Note that DPI induces destabilization only of the free *N*-module, but not of the assembled complex I, similar to what is shown in Fig. 3A. **(E)** Computational modeling of the stability of inter-subunit interactions of isolated *N*-module with or without FMN, one-tail Mann-Whitney *U* test. **(F)** Immunoblot analysis of the effect of 50 nM DPI treatment on *Clpp*$^{-/-}$ MAFs, revealed using antibodies against the *N*-module (left) or against both the *N*- and the Q-module (right). "*" denotes a not fully characterized complex I intermediate which can also be seen in BN gels from Ref. [23]; the authors speculate that this may be a Q/P_P assembly intermediate to which the accumulated NDUFS1 binds.

REACTOME pathways [38] revealed that DPI treatment induces activation of the integrated stress response (ISR), which is similar to previous reports made with other drugs targeting the mitochondrial electron transport chain (mETC) *32*). To assess transcriptional activity based on our transcriptomic data, we employed virtual inference of protein activity by enriched regulon analysis (VIPER) [39] using DoRothEA regulons [40] as a resource for transcription factor-target interactions (Fig. 5B). VIPER analysis identified ATF4 as the transcription factor with the highest score, providing further evidence for the activation of the $eIF_2\alpha$/ISR/ATF4 axis in DPI-treated MAFs. We observed upregulation of genes involved in protein synthesis, tRNA maturation, and amino acid uptake and metabolism (Fig. 5C). Among the upregulated transcripts, we identified several canonical markers of the ATF4-dependent integrated stress response (ISR) (Fig. S2A).

In our analysis, we also found that steroid and cholesterol biosynthesis pathways were significantly downregulated in DPI-treated cells (Fig. 5, A and D). Interestingly, it has been reported that inhibition of complex I can impair the transcriptional activity of Sterol Regulatory Element Binding Transcription Factor 2 (SREBF2) [49,50],. Consistent with this, our VIPER analysis predicted a strong decrease in the transcriptional activity of Srebf1 and Srebf2 (Fig. 5B and Fig. S2, B and C). Overall, the metabolic signature observed is analogous to that described in *vitro* [49,51] and *in vivo* [52–54] models of mitochondrial dysfunction.

Additionally, we observed increased expression of genes involved in mitochondrial import and protein turnover, including *Lonp1*, *Hspa9*, *Hspe1*, and *Hspd1*, which could potentially play a role in the observed degradation of complex I upon DPI treatment (Fig. 5E). We confirmed by Western blot analysis the induction of LONP1, HSPA9, and HSP60 proteins following DPI treatment in human cells (Fig. 5F).

To assess the protein-level changes associated with DPI treatment, we conducted quantitative proteomics analysis using isobaric labeling on DPI-treated cells (Supplementary Data 2). In order to expand our findings beyond MAFs, we employed a human model, the 143 B cancer cell line, which has been extensively used in complex I assembly studies [12,55]. The proteomic analysis confirmed the trends observed in the MAFs transcriptomics analysis: (i) increased levels of proteins involved in the ISR and in mitochondrial protein quality control and (ii) decreased levels of enzymes involved in the cholesterol and mevalonate synthesis pathways (Fig. S2D). Notably, the respiratory complex I subunits were reduced in DPI-treated cells, particularly the *N*-module components (Fig. 5G).

These findings indicate that the degradation of complex I induced by DPI treatment occurs by a post-transcriptional mechanism, in the context of ISR activation. However, it should be noted that although ISR activation and inhibition of cholesterol biosynthesis are characteristic responses to complex I inhibition, they alone do not explain the specific loss of complex I observed with DPI. In fact, other drugs targeting complex I elicit similar responses [49] but do not result in complex I degradation. Therefore, we sought alternative explanations for the observed degradation of complex I.

3.2.4. *DPI treatment induces the loss of complex II*

We made an intriguing observation in our proteomic analysis, as the top downregulated protein was SDHB, an iron-sulfur subunit of complex II (Fig. 5H). Other complex II subunits, namely SDHA, SDHC, and SDHD, were also found to be downregulated, while SDHAF2, an assembly factor involved in the flavination of SDHA, exhibited increased levels (Fig. 5H). These findings contrast with previous studies where complex II subunits were mostly upregulated or unaffected upon complex I deficiency [48].

The stability of complex II was further confirmed to be affected by DPI, particularly when cells were treated for more than 72 h, as evidenced by SDS and BN-gel analyses (Figs. 1E and Fig. 2G and Fig. 5I). This result was surprising considering that DPI is not known to directly inhibit complex II activity (Fig. 5J).

We observed a significant reduction in succinate dehydrogenase

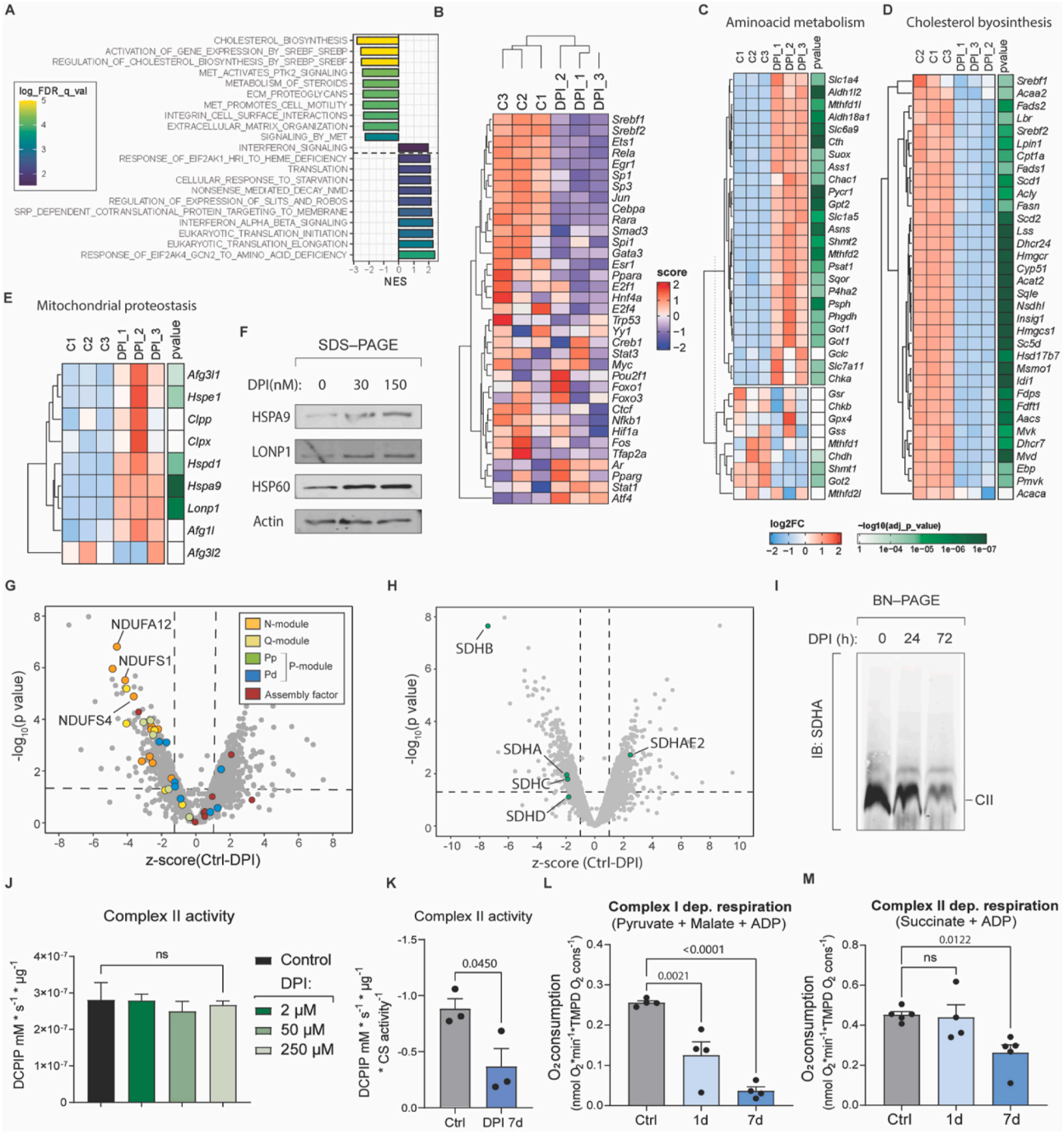

Fig. 5. Transcriptomics and proteomics analysis of DPI treated cells reveals that DPI induces complex II destabilization. (A) GSEA of RNAseq data from 24 h 50 nM DPI treated versus DMSO treated MAFs, n = 3. **(B)** Transcriptional activity of RNAseq data from 24 h 50 nM DPI treated versus DMSO treated cells inferred by VIPER analysis. **(C–E)** Heatmaps of mRNA levels of genes related to amino acid metabolism (C), cholesterol biosynthesis (D) and mitochondrial protein quality control (E) in DPI and DMSO treated MAFs. The log2FC and -log (adjusted p value) legends are the same for each heatmap. **(F)** Immunoblot analysis of mitochondrial proteases and chaperones induction upon 72 h DPI treatment in 143 B cells. **(G–H)** Volcano plot analysis of proteomics results obtained by comparing 50 nM DPI- vs DMSO-treated 143 B cells highlighting complex I subunits and assembly factors (G) and complex II subunits (H), n = 3. **(I)** Immunoblot analysis of the effect of 50 nM DPI on complex II. **(J)** Complex II activity of isolated mitochondria from mouse kidney treated *in vitro* with DPI. **(K)** Complex II activity, normalized on CS activity, of isolated mitochondria from cells treated with 50 nM DPI for 7 days. **(L, M)** Analysis of coupled respiration of permeabilized cells treated with 50 nM DPI for either one day or one week assessed with complex I (L) or complex II (M) substrates. Data represented as mean ± S.E.M., ordinary two-way ANOVA, Dunnett's multiple comparisons test (I, L, M); two-tail upaired *t*-test (K).

(SDH) activity in mitochondria extracted from MAFs treated with DPI for 7 days, which amounted to a 60 % decrease compared to the control group (Fig. 5K). Additionally, both complex I and complex II-dependent oxygen consumption showed a decline in cells incubated with DPI for 7 days, whereas in cells treated for only 1 day, the impairment was limited to complex I-dependent respiration (Fig. 5, L and M). The activity of complex IV and the citrate synthase enzyme remained unaltered under the same conditions (Fig. S2, E and F). These findings provide evidence that prolonged exposure to DPI leads to the loss of both complex I and complex II.

3.2.4.1. DPI depletes mitochondrial FMN pool. Our hypothesis was that DPI affects the stability of both complex I and complex II through a shared mechanism. Both complexes rely on flavin cofactors, with complex I utilizing FMN and complex II utilizing FAD. It is known that flavoproteins lacking bound cofactors may be targeted for degradation by protein quality control systems [19,56]. Since DPI is recognized as an inhibitor of various flavoproteins [57] and has the ability to react with reduced flavins in solution [44], we speculated that the loss of complex I could be attributed to the depletion of the mitochondrial flavin cofactor pool caused by DPI.

We found that cells treated with DPI for 24 h exhibited a significant reduction of 43 % in flavin-specific fluorescence compared to untreated cells or cells treated with rotenone (Fig. 6A). Additionally, when isolated mitochondria were treated with DPI *in vitro*, a dose-dependent decrease in flavin-specific fluorescence was observed (Fig. 6B). To further investigate the impact of DPI on flavin cofactors, we analyzed the levels of riboflavin, FMN, and FAD in isolated cytosolic and mitochondrial fractions from DPI-treated 143 B cells using HPLC (Fig. 6C and D, and Fig. S3A). DPI treatment resulted in a decrease of the three cofactors in both compartments, with FMN concentration showing a reduction of 28 % in the cytosol and 49 % in mitochondria. Interestingly, FAD decreased much more in the cytosol than in mitochondria. These findings demonstrate that DPI treatment leads to depletion of FAD and FMN in cells.

When MAFs were grown in riboflavin-free media, a significant decrease in the levels of complex I and complex II was observed, confirming the crucial role of the cofactor in the stability of respiratory flavoenzymes (Fig. 6E). Additionally, in clear-native gels, which allow direct visualization of flavoenzyme fluorescence without the interference of Coomassie dye, cells grown in riboflavin-deficient medium exhibited a substantial reduction in flavoprotein fluorescence (Fig. 6F). Similar fluorescence reduction was observed for complex I in MAFs treated with DPI (Fig. 6G). Furthermore, both DPI treatment and riboflavin depletion led to a decrease in the amount of complex I subunits (Fig. 6H and Fig. S3B). ACAD9, a flavoprotein involved in complex I assembly and known to be associated with riboflavin-responsive complex I deficiency in humans, also showed reduced levels (Fig. 6H and Fig. S3B).

SIL-based proteomic analysis conducted on human 143 B cells grown in riboflavin-free medium corroborated our findings from the

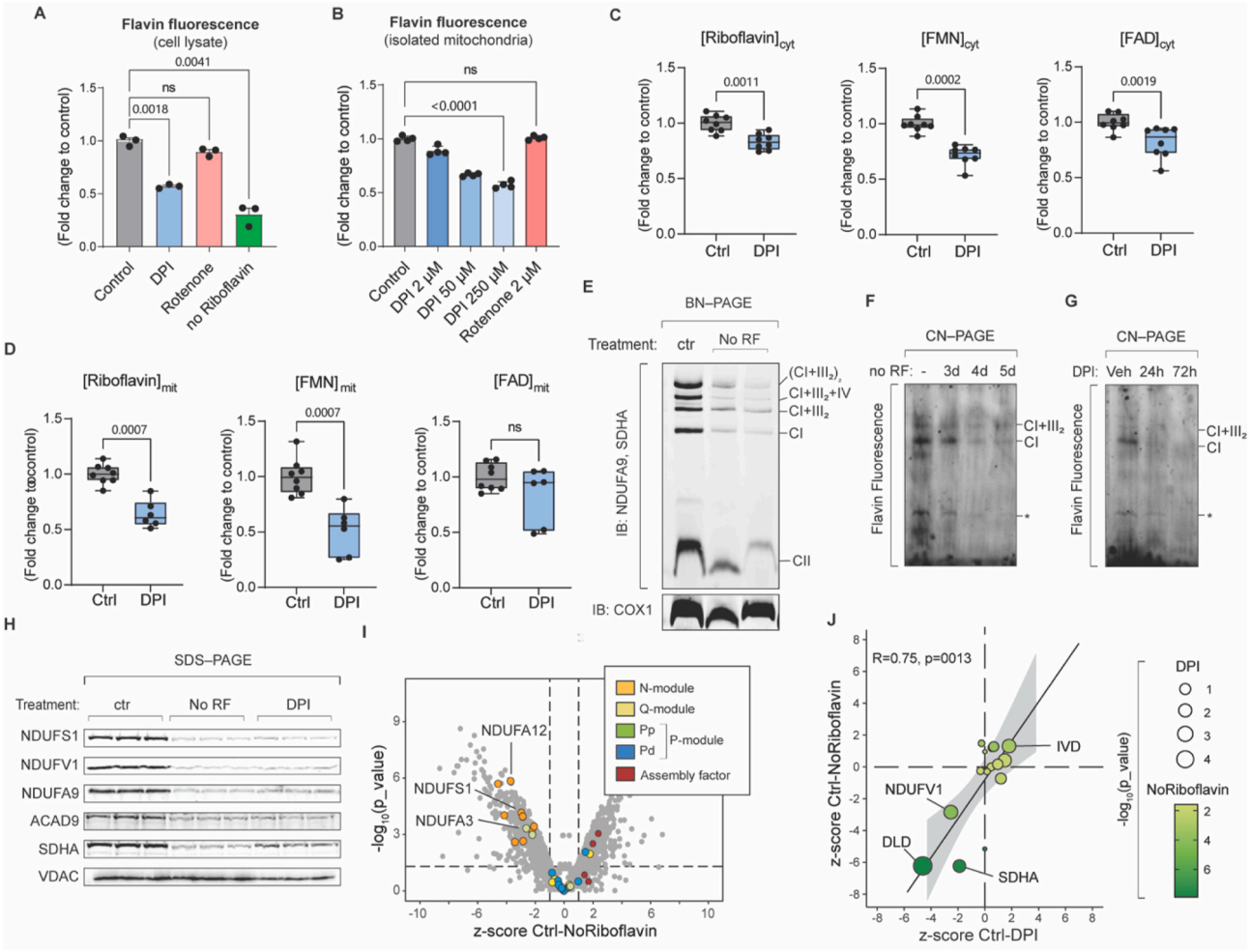

Fig. 6. DPI depletes mitochondria of FMN to destabilize complex I. (A, B) Analysis of total flavin fluorescence of MAFs (A) and isolated kidney mitochondria (B) treated with either 400 nM DPI, rotenone or DMSO for 48 h, ordinary two-way ANOVA, Dunnett's multiple comparisons test. **(C, D)** Quantification of riboflavin, FMN and FAD content in the cytosolic (C) and mitochondrial (D) fractions of 143 B cells treated either with DMSO or 400 nM DPI for 48 h, Mann-Whitney two-tailed test. **(E)** Immunoblot analysis of the effect of riboflavin deficiency on the supramolecular organization of complex I and complex II in MAFs. **(F, G)** In-gel flavin fluorescence detection of mitochondria isolated from riboflavin-depleted (F) or DPI-treated (G) MAFs. *: unknown flavoprotein. **(H)** Immunoblot analysis of the effect of DPI and riboflavin-deficiency on complex I and complex II subunits abundance relative to VDAC. The quantification is displayed in Fig. S3B. **(I)** Volcano plot analysis of proteomics results obtained by comparing 143 B cells grown in normal vs riboflavin-depleted media highlighting complex I subunits and assembly factors, n = 3. **(J)** Correlation between the effects of DPI and of riboflavin deficiency on the abundance of matrix flavoproteins assessed by proteomics. Data represented as mean ± S.E.M.

immunoblot analysis (Fig. 6I and Fig. S3C). The subunits of complex I, particularly those belonging to the *N*-module, were predominantly affected by the riboflavin deficiency. When we compared the impact of DPI treatment and riboflavin deficiency on other mitochondrial matrix flavoproteins, we observed a correlation between the two treatments (Pearson's R = 0.75, p = 0.0013, Fig. 6J). The protein abundance of dihydrolipoamide dehydrogenase (DLD), a FAD-dependent component of various mitochondrial dehydrogenases, was decreased along with NDUFV1 and SDHA. However, the abundance of many other matrix flavoenzymes remained unchanged, suggesting that both treatments induce a common degradation mechanism directed only towards certain flavoproteins in the mitochondrial matrix.

To support the relationship between riboflavin and complex I, we reanalyzed proteomics data from a previous study conducted on the murine melanoma cell line B16, where cells were cultured in the absence of riboflavin for 3 days [19]. Consistent with our findings, the levels of complex I subunits were primarily reduced, with a notable decrease observed in the *N*-module subunits (Fig. S3D).

Overall, these findings provide strong evidence for the regulatory role of FMN in the biogenesis and stability of respiratory complex I in mammalian cells. They also indicate that the complete loss of complex I induced by long-term DPI treatment is caused by the depletion of intracellular FMN pool.

3.2.5. *SLC25A32 knockout impairs complex I stability and function*

To further investigate the impact of mitochondrial flavin shortage on complex I stability and activity, we utilized CRISPR/Cas9 technology to knock out the *SLC25A32* gene, which encodes the mitochondrial flavin carrier responsible for transporting FAD into the mitochondrial matrix [58,59]. Once in the mitochondria, FAD is converted into FMN by the mitochondrial isoform of the FAD synthase [60]. We generated *SLC25A32* knockout (KO) clones in 143 B cells, with a clone expressing a non-targeting sgRNA serving as the control. In SLC25A32^{KO} cells, the flavin-specific fluorescence of mitochondria was reduced compared to cells expressing the non-targeting sgRNA, indicating a decrease in mitochondrial flavin content (Fig. 7A). BN-gel analysis further confirmed that the total amount of complex I was decreased in the SLC25A32^{KO} cells, supporting the role of the FMN cofactor in complex I stability (Fig. 7B and C). Moreover, the SLC25A32^{KO} cells exhibited a decrease in complex I isolated activity (Fig. 7D) as well as in complex I and complex II-dependent respiration (Fig. 7E). These findings suggest that perturbation of mitochondrial transport and metabolism of flavin cofactors, as observed in the SLC25A32^{KO} cells, leads to destabilization of complex I and impairment of its activity, highlighting the importance of proper flavin homeostasis for complex I function.

4. Discussion

The study of respiratory complex I inhibition has gained significant attention due to its potential therapeutic applications in various prevalent diseases [2,8]. Current research focuses on drugs that target the quinone binding pocket (Q-site) of complex I [3,4], while only a limited number of compounds are known to target the *N*-site of the enzyme [20,61,62]. For this reason, the specific cellular responses elicited by *N*-site inhibitors remain largely unexplored. In this context, we investigated the properties of DPI, a known inhibitor of complex I at the *N*-site. Our

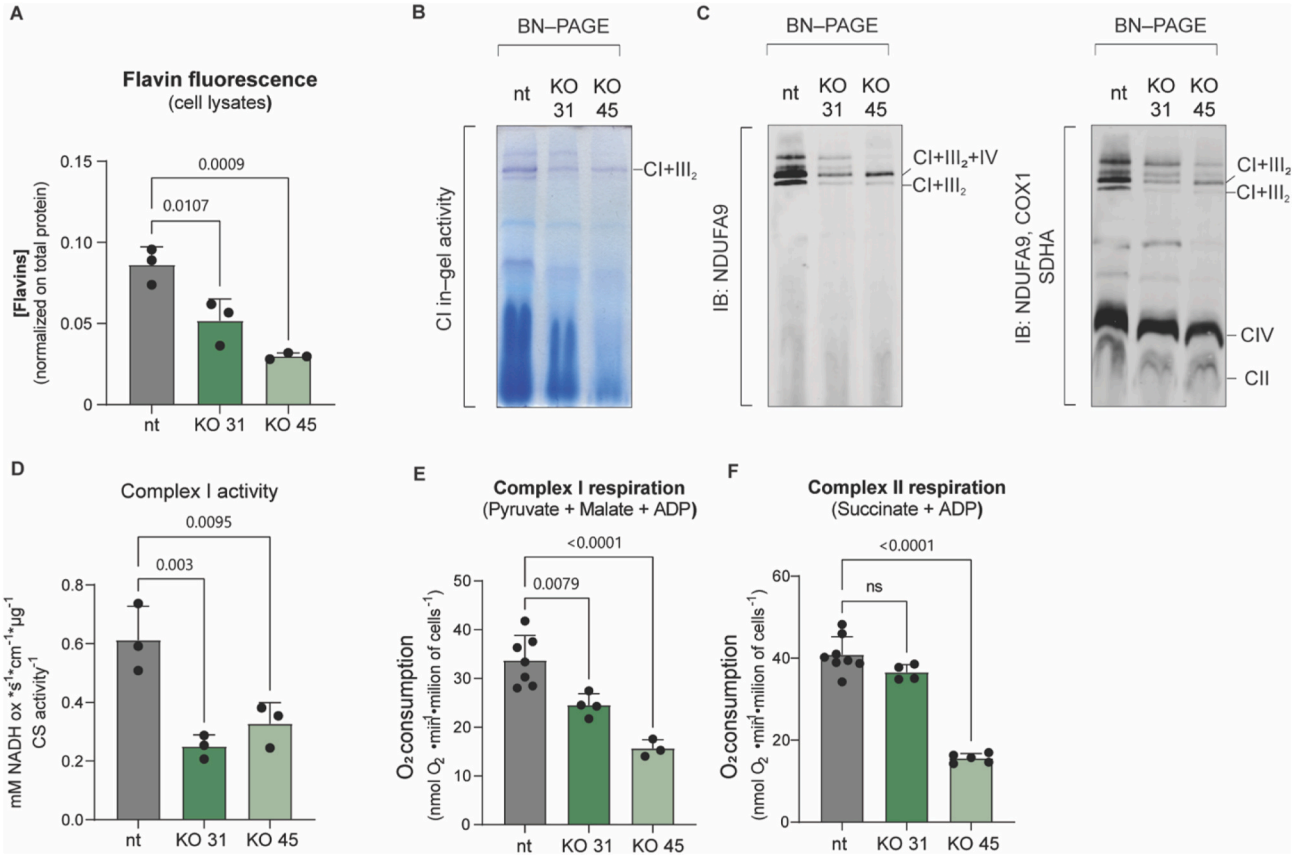

Fig. 7. SLC25A32 knockout impairs complex I stability and function. (A) Analysis of flavin fluorescence of isolated mitochondria from SLC25A32^{KO} cells. **(B)** In-gel analysis of complex I activity in SLC25A32^{KO} cells (human cells lack the most prominent complex I band that is normally seen in mouse cells). **(C)** Immunoblot analysis of the supramolecular organization of complex I in SLC25A32^{KO} cells. **(D)** Complex I activity, normalized on CS activity, of isolated mitochondria from SLC25A32^{KO} cells. **(E, F)** Analysis of coupled respiration of permeabilized SLC25A32^{KO} cells assessed with complex I (E) or complex II (F) substrates. Data represented as mean ± S.E.M., ordinary two-way ANOVA, Dunnett's multiple comparisons test.

findings revealed that DPI possesses unique characteristics that make it a valuable tool for studying unexplored aspects of complex I biology both *in vitro* and *in vivo*.

DPI has been found to react covalently with riboflavin, FMN, and FAD in solution, resulting in the formation of inactive flavin-phenyl adducts [44]. This reaction mechanism has been well-described in studies focusing on the inhibition of isolated flavoenzymes by DPI [20,57,63,64]. However, it is often overlooked in studies conducted with live cells, where DPI is primarily used as a NOX-inhibitor [65]. As a result, the impact of DPI on cellular and mitochondrial flavin levels has not been extensively considered. Additionally, it should be noted that DPI is a lipophilic cation, which likely facilitates its accumulation within mitochondria. This accumulation in mitochondria can explain why DPI is capable of arresting cell growth in galactose at low concentrations but requires much higher doses (in the micromolar range) to inhibit complex I *in vitro* [20].

The interaction of DPI with FMN within the mitochondria leads to the stabilization of FMN in its reduced state [20]. In this reduced form ($FMNH_2$), FMN has a significantly lower affinity for its binding site compared to the oxidized form (FMN). As a result, $FMNH_2$ tends to dissociate from the enzyme [66]. The dissociation of FMN from mature complex I is reversible in the context of the whole enzyme both in bacteria and in mitochondria, and does not cause dramatic structural changes [67,68]. However, it has been shown that the dissociation of FMN from the isolated *N*-module can lead to its irreversible denaturation [66,69], in accordance with our results. This observation provides a potential explanation for recent findings that highlight the synthesis of *N*-module subunits in a large excess and independently of the rest of the complex [23].

During the turnover of the physiological complex I, assembly intermediates typically do not accumulate since they are promptly integrated into the nascent complex [12]. However, this is not true in several pathological situations that disturb complex I assembly and maintenance. For example, in patients with mutations in nuclear-encoded *N*-module subunits [46,47], a distinct Q/P subcomplex is observed. We observed the accumulation of the same subcomplex in tissues of mice treated with DPI. Therefore, the accumulation of a Q/P subcomplex may serve as indication of *N*-module dysfunction. One possibility is that the presence of an enzymatically active FMN is necessary for the completion of complex I maturation to prevent the formation of dysfunctional complex I, which could potentially result in excessive production of ROS. Recently, a mitochondrial leucine-tyrosine-arginine motif containing protein, LYRM2, has been shown to be important for *N*-module assembly [70]. An intriguing explanation proposed by the authors is that LYRM2 may mediate the incorporation of FMN into the *N*-module.

The unexpected impact of long-term DPI treatment on complex I highlights the crucial requirement for a continuous supply of flavin to maintain complex I stability within the mitochondria. When riboflavin is scarce, complex I and complex II subunits undergo degradation via a post-translational mechanism regulated by multiple layers of control. Protein quality control machineries plays a role in recognizing and eliminating numerous enzymes lacking FAD to prevent the formation of protein aggregates [17–19]. For instance, in the absence of its cofactor, the cytosolic flavoprotein NQO1 undergoes ubiquitination by the E3 ubiquitin-protein ligase CHIP and subsequent removal [18,19]. We hypothesize that a similar quality control mechanism operates within the mitochondrial matrix, where the absence of FMN likely renders complex I subunits susceptible to degradation by the mitochondrial proteolytic machinery. Indeed, we observed an upregulation of various genes involved in mitochondrial proteostasis such as *LONP1,* which has been shown to degrade complex I subunits in response to membrane depolarization [71] and to decrease the levels of core complex I subunits upon overexpression [72]. Interestingly, among the 43 flavoproteins active in the mitochondrial matrix [10], complex I stands out as the only one utilizing FMN instead of FAD. The underlying reasons for this distinct preference have yet to be explored; nevertheless, it opens up possibilities for selective regulatory mechanisms governing mitochondrial FAD and FMN availability. The precise molecular characterization of the flavin-dependent protein quality control of the mitochondrial matrix is a compelling avenue for future research.

Another factor contributing to the unique sensitivity of complex I to mitochondrial flavin supply is the reliance on FAD-dependent assembly factors, namely FOXRED1 and ACAD9, for complex I assembly [73,74]. Patients with mutations in the ACAD9 gene often develop complex I deficiency, which can be alleviated through riboflavin supplementation [14]. We observed reduced levels also of ACAD9 following both DPI treatment and riboflavin depletion, indicating that the assembly machinery of complex I is regulated by mitochondrial FAD. Therefore, our findings provide further support for the rationale behind riboflavin supplementation in the treatment of patients afflicted with complex I deficiency [75].

As of now, no mitochondrial FMN transporter has been described, leading to the proposal of two mechanisms to explain the origin of mitochondrial FMN: (i) the import of riboflavin and subsequent synthesis of FMN by mitochondrial riboflavin kinase [76], and/or (ii) the import of FAD followed by hydrolysis to FMN by mitochondrial FAD synthase [60]. To further establish the connection between mitochondrial flavin supply and complex I stability, we conducted knockout experiments on *SLC25A32*, the gene encoding the mitochondrial FAD transporter. While SLC25A32 was originally identified as a folate carrier [77], new data from genetic mouse models indicates that the folate metabolism defects are secondary to mitochondrial FAD deficiency [58]. In humans, mutations in *SLC25A32* result in a range of disorders that exhibit a positive response to riboflavin treatment [78]. Our $SLC25A32^{KO}$ cells demonstrated a reduction in the mitochondrial flavin pool, as well as diminished assembly and activity of complex I, which confirms our previous findings. Interestingly, despite the absence of *SLC25A32*, mitochondria from these cells still contained residual flavin cofactors and retained some level of complex I activity. This observation aligns with data obtained from mice carrying pathological mutations in the *SLC25A32* gene, where riboflavin uptake by mitochondria remained unaffected despite the severe FAD transport defect [58]. In other words, mitochondria lacking *SLC25A32* are still capable of importing riboflavin. Together, our study and these findings, support the notion of redundant mechanisms for mitochondrial riboflavin transport, the specific molecular identity of which has been a subject of debate [11]. Recent advancements have identified mitochondrial transporters for NAD^+ [79–81]and glutathione [82,83]. We believe that the data presented here will encourage further research to identify alternative mitochondrial riboflavin carriers.

Taken together, these findings establish a strong connection between complex I stability and its organic cofactor, FMN, implying that the regulation of mitochondrial FMN levels could be an unexplored avenue for controlling respiratory complex I levels. Moreover, our research indicates that the utilization of DPI could be valuable in the development of alternative approaches to modulate complex I activity and mitigate pathological ROS production in diverse clinical scenarios.

Funding

This study was supported by grants from Ministerio de Ciencia e Innovación [grants PID2021-127988OB-I00 & TED2021-131611B-100], Human Frontier Science Program [grant RGP0016/2018], Fundación Leduq [17CVD04] Instituto de Salud Carlos III CIBERFES [CB16/10/00282] to JAE. Ministerio de Ciencia e Innovación MCIN/AEI/1013039/501100011033 [PID2022-136369NB-I00] and Government of Aragón-FEDER [E35_23R] to MM. Ministerio de Ciencia e Innovación [PID2021-122348NB-I00, PLEC2022-009235 and PLEC2022-009298] Comunidad de Madrid (IMMUNO-VAR, P2022/BMD-7333) and "la Caixa" Banking Foundation (project codes HR17-00247 and HR22-00253) to JV. AC was supported by the European Union's Horizon 2020 research and innovation program under the Marie Skłodowska-Curie

grant agreement n. 713,673.

MRM is supported by a Ministerio de Ciencia e Inovación Fellowship [FPI-SO-2021:PRE2021-097,721]. The CNIC is supported by the Instituto de Salud Carlos III (ISCIII), the Ministerio de Ciencia e Innovación (MCIN) and the Pro CNIC Foundation, and is a Severo Ochoa Center of Excellence (grant CEX2020-001041-S funded by MICIN/AEI/1,013,039/501,100,011,033).

Author contributions

Conceptualization: AC and JAE. CRISPR KO, respirometry, fluorescence, enzymatic activity, data analysis and *in vivo* experiments: AC. Mitochondrial isolation, BN-gel and immunoblot analysis: AC and AG. Quantitative analyses of RNAseq data and computational support: JLC. Computational modeling experiments: MRM, JLC. HPLC-based quantification of flavins: MR, MM. Proteomics analyses: EC, JV. Visualization: AC. Writing: AC and JAE with inputs from all authors.

Data and materials availability

RNA-seq data are available at GEO (GSE249118) and proteomics data at PRIDE (PXD047527). See also Supplementary Data 1 and 2.

Declaration of competing interest

The authors declare no competing interests.

Data availability

Data are available in GEO and PRIDE.

Acknowledgments

We acknowledge all GENOXPHOS group members for their scientific discussions contributing to this manuscript. We thank Dr. Aleksandra Ttrifunovic for providing Clpp-deficient MAFs. We thank Maria Barile for the precious suggestions on flavin analysis. We thank members of the CNIC facilities (Genomics, Bioinformatics, Cell culture, Animal facility and Viral vectors) for their technical assistance.

Appendix A. Supplementary data

Supplementary data to this article can be found online at https://doi.org/10.1016/j.redox.2023.103001.

References

[1] M.D. Brand, R.L.S. Goncalves, A.L. Orr, L. Vargas, A.A. Gerencser, M. Borch Jensen, Y.T. Wang, S. Melov, C.N. Turk, J.T. Matzen, V.J. Dardov, H.M. Petrassi, S. L. Meeusen, I.V. Perevoshchikova, H. Jasper, P.S. Brookes, E.K. Ainscow, Suppressors of superoxide-H2O2 production at site IQ of Citochondrial complex I protect against stem cell hyperplasia and ischemia-reperfusion injury, Cell Metabol. 24 (2016) 582–592.

[2] J.R. Molina, Y. Sun, M. Protopopova, S. Gera, M. Bandi, C. Bristow, T. McAfoos, P. Morlacchi, J. Ackroyd, A.-N.A. Agip, G. Al-Atrash, J. Asara, J. Bardenhagen, C. C. Carrillo, C. Carroll, E. Chang, S. Ciurea, J.B. Cross, B. Czako, A. Deem, N. Daver, J.F. de Groot, J.-W. Dong, N. Feng, G. Gao, J. Gay, M.G. Do, J. Greer, V. Giuliani, J. Han, L. Han, V.K. Henry, J. Hirst, S. Huang, Y. Jiang, Z. Kang, T. Khor, S. Konoplev, Y.-H. Lin, G. Liu, A. Lodi, T. Lofton, H. Ma, M. Mahendra, P. Matre, R. Mullinax, M. Peoples, A. Petrocchi, J. Rodriguez-Canale, R. Serreli, T. Shi, M. Smith, Y. Tabe, J. Theroff, S. Tiziani, Q. Xu, Q. Zhang, F. Muller, R.A. DePinho, C. Toniatti, G.F. Draetta, T.P. Heffernan, M. Konopleva, P. Jones, M.E. Di Francesco, J.R. Marszalek, An inhibitor of oxidative phosphorylation exploits cancer vulnerability, Nat. Med. 24 (2018) 1036–1046.

[3] H.R. Bridges, J.N. Blaza, Z. Yin, I. Chung, M.N. Pollak, J. Hirst, Structural basis of mammalian respiratory complex I inhibition by medicinal biguanides, Science 379 (2023) 351–357.

[4] I. Chung, R. Serreli, J.B. Cross, M.E. Di Francesco, J.R. Marszalek, J. Hirst, Cork-in-bottle mechanism of inhibitor binding to mammalian complex I, Sci. Adv. 7 (2021), eabg4000.

[5] H.R. Bridges, J.G. Fedor, J.N. Blaza, A. Di Luca, A. Jussupow, O.D. Jarman, J. J. Wright, A.-N.A. Agip, A.P. Gamiz-Hernandez, M.M. Roessler, V.R.I. Kaila, J. Hirst, Structure of inhibitor-bound mammalian complex I, Nat. Commun. 11 (2020) 5261.

[6] J. Hirst, Mitochondrial complex I, Annu. Rev. Biochem. 82 (2013) 551–575.

[7] F. Scialò, A. Sriram, D. Fernández-Ayala, N. Gubina, M. Lõhmus, G. Nelson, A. Logan, H.M. Cooper, P. Navas, J.A. Enríquez, M.P. Murphy, A. Sanz, Mitochondrial ROS produced via reverse electron transport extend animal lifespan, Cell Metabol. 23 (2016) 725–734.

[8] E.T. Chouchani, V.R. Pell, E. Gaude, D. Aksentijević, S.Y. Sundier, E.L. Robb, A. Logan, S.M. Nadtochiy, E.N.J. Ord, A.C. Smith, F. Eyassu, R. Shirley, C.-H. Hu, A. J. Dare, A.M. James, S. Rogatti, R.C. Hartley, S. Eaton, A.S.H. Costa, P.S. Brookes, S.M. Davidson, M.R. Duchen, K. Saeb-Parsy, M.J. Shattock, A.J. Robinson, L. M. Work, C. Frezza, T. Krieg, M.P. Murphy, Ischaemic accumulation of succinate controls reperfusion injury through mitochondrial ROS, Nature 515 (2014) 431–435.

[9] V. Massey, The chemical and biological versatility of riboflavin, Biochem. Soc. Trans. 28 (2000) 283–296.

[10] W.-D. Lienhart, V. Gudipati, P. Macheroux, The human flavoproteome, Arch. Biochem. Biophys. 535 (2013) 150–162.

[11] A. Curtabbi, J.A. Enríquez, The ins and outs of the flavin mononucleotide cofactor of respiratory complex I, IUBMB Life 74 (2022) 629–644.

[12] S. Guerrero-Castillo, F. Baertling, D. Kownatzki, H.J. Wessels, S. Arnold, U. Brandt, L. Nijtmans, The assembly pathway of mitochondrial respiratory chain complex I, Cell Metabol. 25 (2017) 128–139.

[13] F. Varghese, E. Atcheson, H.R. Bridges, J. Hirst, Characterization of clinically identified mutations in NDUFV1, the flavin-binding subunit of respiratory complex I, using a yeast model system, Hum. Mol. Genet. 24 (2015) 6350–6360.

[14] B.M. Repp, E. Mastantuono, C.L. Alston, M. Schiff, T.B. Haack, A. Rötig, A. Ardissone, A. Lombès, C.B. Catarino, D. Diodato, G. Schottmann, J. Poulton, A. Burlina, A. Jonckheere, A. Munnich, B. Rolinski, D. Ghezzi, D. Rokicki, D. Wellesley, D. Martinelli, D. Wenhong, E. Lamantea, E. Ostergaard, E. Pronicka, G. Pierre, H.J.M. Smeets, I. Wittig, I. Scurr, I.F.M. de Coo, I. Moroni, J. Smet, J. A. Mayr, L. Dai, L. de Meirleir, M. Schuelke, M. Zeviani, R.J. Morscher, R. McFarland, S. Seneca, T. Klopstock, T. Meitinger, T. Wieland, T.M. Strom, U. Herberg, U. Ahting, W. Sperl, M.-C. Nassogne, H. Ling, F. Fang, P. Freisinger, R. Van Coster, V. Strecker, R.W. Taylor, J. Häberle, J. Vockley, H. Prokisch, S. Wortmann, Clinical, biochemical and genetic spectrum of 70 patients with ACAD9 deficiency: is riboflavin supplementation effective? Orphanet J. Rare Dis. 13 (2018) 120.

[15] M. Bar-Meir, O.N. Elpeleg, A. Saada, Effect of various agents on adenosine triphosphate synthesis in mitochondrial complex I deficiency, J. Pediatr. 139 (2001) 868–870.

[16] H.R. Scholte, H.F. Busch, H.D. Bakker, J.M. Bogaard, I.E. Luyt-Houwen, L.P. Kuyt, Riboflavin-responsive complex I deficiency, Biochim. Biophys. Acta 1271 (1995) 75–83.

[17] T. Saijo, K. Tanaka, Isoalloxazine ring of FAD is required for the formation of the core in the Hsp60-assisted folding of medium chain acyl-CoA dehydrogenase subunit into the assembly competent conformation in mitochondria, J. Biol. Chem. 270 (1995) 1899–1907.

[18] O. Moscovitz, P. Tsvetkov, N. Hazan, I. Michaelevski, H. Keisar, G. Ben-Nissan, Y. Shaul, M. Sharon, A mutually inhibitory feedback loop between the 20S proteasome and its regulator, NQO1. Molecular Cell 47 (2012) 76–86.

[19] A. Martínez-Limón, M. Alriquet, W.-H. Lang, G. Calloni, I. Wittig, R.M. Vabulas, Recognition of enzymes lacking bound cofactor by protein quality control, Proc. Natl. Acad. Sci. USA 113 (2016) 12156–12161.

[20] A. Majander, M. Finel, M. Wikström, Diphenyleneiodonium inhibits reduction of iron-sulfur clusters in the mitochondrial NADH-ubiquinone oxidoreductase (Complex I), J. Biol. Chem. 269 (1994) 21037–21042.

[21] R. Moreno-Loshuertos, R. Acín-Pérez, P. Fernández-Silva, N. Movilla, A. Pérez-Martos, S. Rodriguez de Cordoba, M.E. Gallardo, J.A. Enríquez, Differences in reactive oxygen species production explain the phenotypes associated with common mouse mitochondrial DNA variants, Nat. Genet. 38 (2006) 1261–1268.

[22] J. Dutil, Z. Chen, A.N. Monteiro, J.K. Teer, S.A. Eschrich, An interactive resource to probe genetic diversity and estimated ancestry in cancer cell lines, Cancer Res. 79 (2019) 1263–1273.

[23] K. Szczepanowska, K. Senft, J. Heidler, M. Herholz, A. Kukat, M.N. Höhne, E. Hofsetz, C. Becker, S. Kaspar, H. Giese, K. Zwicker, S. Guerrero-Castillo, L. Baumann, J. Kauppila, A. Rumyantseva, S. Müller, C.K. Frese, U. Brandt, J. Riemer, I. Wittig, A. Trifunovic, A salvage pathway maintains highly functional respiratory complex I, Nat. Commun. 11 (2020) 1643.

[24] P. Leone, M. Tolomeo, M. Barile, Continuous and discontinuous approaches to study FAD synthesis and degradation catalyzed by purified recombinant FAD synthase or cellular fractions, Methods Mol. Biol. 2280 (2021) 87–116.

[25] F. Ansari, B. Yoval-Sánchez, Z. Niatsetskaya, S. Sosunov, A. Stepanova, C. Garcia, E. Owusu-Ansah, V. Ten, I. Wittig, A. Galkin, Quantification of NADH:ubiquinone oxidoreductase (complex I) content in biological samples, J. Biol. Chem. 297 (2021), https://doi.org/10.1016/j.jbc.2021.101204.

[26] A. Serrano, S. Frago, B. Herguedas, M. Martínez-Júlvez, A. Velázquez-Campoy, M. Medina, Key residues at the riboflavin kinase catalytic site of the bifunctional riboflavin kinase/FMN adenylyltransferase from Corynebacterium ammoniagenes, Cell Biochem. Biophys. 65 (2013) 57–68.

[27] I. Wittig, H.-P. Braun, H. Schägger, Blue native PAGE, Nat. Protoc. 1 (2006) 418–428.

[28] F.A. Ran, P.D. Hsu, J. Wright, V. Agarwala, D.A. Scott, F. Zhang, Genome engineering using the CRISPR-Cas9 system, Nat. Protoc. 8 (2013) 2281–2308.

[29] CHOPCHOP, (available at: https://chopchop.cbu.uib.no/).

[30] S. Martínez-Bartolomé, P. Navarro, F. Martín-Maroto, D. López-Ferrer, A. Ramos-Fernández, M. Villar, J.P. García-Ruiz, J. Vázquez, Properties of average score distributions of SEQUEST: the probability ratio method, Mol. Cell. Proteomics 7 (2008) 1135–1145.

[31] P. Navarro, M. Trevisan-Herraz, E. Bonzon-Kulichenko, E. Núñez, P. Martínez-Acedo, D. Pérez-Hernández, I. Jorge, R. Mesa, E. Calvo, M. Carrascal, M. L. Hernáez, F. García, J.A. Bárcena, K. Ashman, J. Abian, C. Gil, J.M. Redondo, J. Vázquez, General statistical framework for quantitative proteomics by stable isotope labeling, J. Proteome Res. 13 (2014) 1234–1247.

[32] F. García-Marqués, M. Trevisan-Herraz, S. Martínez-Martínez, E. Camafeita, I. Jorge, J.A. Lopez, N. Méndez-Barbero, S. Méndez-Ferrer, M.A. Del Pozo, B. Ibáñez, V. Andrés, F. Sánchez-Madrid, J.M. Redondo, E. Bonzon-Kulichenko, J. Vázquez, A novel systems-biology Algorithm for the analysis of coordinated protein responses using quantitative proteomics, Mol. Cell. Proteomics 15 (2016) 1740–1760.

[33] B. Li, C.N. Dewey, RSEM: accurate transcript quantification from RNA-Seq data with or without a reference genome, BMC Bioinf. 12 (2011) 323.

[34] M.D. Robinson, A. Oshlack, A scaling normalization method for differential expression analysis of RNA-seq data, Genome Biol. 11 (2010) R25.

[35] C.W. Law, Y. Chen, W. Shi, G.K. Smyth, voom: precision weights unlock linear model analysis tools for RNA-seq read counts, Genome Biol. 15 (2014) R29.

[36] A. Subramanian, P. Tamayo, V.K. Mootha, S. Mukherjee, B.L. Ebert, M.A. Gillette, A. Paulovich, S.L. Pomeroy, T.R. Golub, E.S. Lander, J.P. Mesirov, Gene set enrichment analysis: a knowledge-based approach for interpreting genome-wide expression profiles, Proc. Natl. Acad. Sci. USA 102 (2005) 15545–15550.

[37] V.K. Mootha, C.M. Lindgren, K.-F. Eriksson, A. Subramanian, S. Sihag, J. Lehar, P. Puigserver, E. Carlsson, M. Ridderstråle, E. Laurila, N. Houstis, M.J. Daly, N. Patterson, J.P. Mesirov, T.R. Golub, P. Tamayo, B. Spiegelman, E.S. Lander, J. N. Hirschhorn, D. Altshuler, L.C. Groop, PGC-1α-responsive genes involved in oxidative phosphorylation are coordinately downregulated in human diabetes, Nat. Genet. 34 (2003) 267–273.

[38] M. Gillespie, B. Jassal, R. Stephan, M. Milacic, K. Rothfels, A. Senff-Ribeiro, J. Griss, C. Sevilla, L. Matthews, C. Gong, C. Deng, T. Varusai, E. Ragueneau, Y. Haider, B. May, V. Shamovsky, J. Weiser, T. Brunson, N. Sanati, L. Beckman, X. Shao, A. Fabregat, K. Sidiropoulos, J. Murillo, G. Viteri, J. Cook, S. Shorser, G. Bader, E. Demir, C. Sander, R. Haw, G. Wu, L. Stein, H. Hermjakob, P. D'Eustachio, The reactome pathway knowledgebase 2022, Nucleic Acids Res. 50 (2022) D687–D692.

[39] M.J. Alvarez, Y. Shen, F.M. Giorgi, A. Lachmann, B.B. Ding, B.H. Ye, A. Califano, Functional characterization of somatic mutations in cancer using network-based inference of protein activity, Nat. Genet. 48 (2016) 838–847.

[40] L. Garcia-Alonso, C.H. Holland, M.M. Ibrahim, D. Turei, J. Saez-Rodriguez, Benchmark and integration of resources for the estimation of human transcription factor activities, Genome Res. 29 (2019) 1363–1375.

[41] Z. Gu, Complex heatmap visualization, iMeta 1 (2022) e43.

[42] M. Degli Esposti, Inhibitors of NADH-ubiquinone reductase: an overview, Biochim. Biophys. Acta 1364 (1998) 222–235.

[43] A. Guarás, E. Perales-Clemente, E. Calvo, R. Acín-Pérez, M. Loureiro-Lopez, C. Pujol, I. Martínez-Carrascoso, E. Nuñez, F. García-Marqués, M.A. Rodríguez-Hernández, A. Cortés, F. Diaz, A. Pérez-Martos, C.T. Moraes, P. Fernández-Silva, A. Trifunovic, P. Navas, J. Vazquez, J.A. Enríquez, The CoQH2/CoQ ratio serves as a sensor of respiratory chain efficiency, Cell Rep. 15 (2016) 197–209.

[44] S. Chakraborty, V. Massey, Reaction of reduced flavins and flavoproteins with diphenyliodonium chloride, J. Biol. Chem. 277 (2002) 41507–41516.

[45] M.J.W. Adjobo-Hermans, R. de Haas, P.H.G.M. Willems, A. Wojtala, S.E. van Emst-de Vries, J.A. Wagenaars, M. van den Brand, R.J. Rodenburg, J.A.M. Smeitink, L. G. Nijtmans, L.A. Sazanov, M.R. Wieckowski, W.J.H. Koopman, NDUFS4 deletion triggers loss of NDUFA12 in Ndufs4-/- mice and Leigh syndrome patients: a stabilizing role for NDUFAF2, Biochim. Biophys. Acta Bioenerg. 1861 (2020), 148213.

[46] S.J.G. Hoefs, O.H. Skjeldal, R.J. Rodenburg, B. Nedregaard, E.P.M. van Kaauwen, U. Spiekerkötter, J.-C. von Kleist-Retzow, J.A.M. Smeitink, L.G. Nijtmans, L.P. van den Heuvel, Novel mutations in the NDUFS1 gene cause low residual activities in human complex I deficiencies, Mol. Genet. Metabol. 100 (2010) 251–256.

[47] M. Lazarou, M. McKenzie, A. Ohtake, D.R. Thorburn, M.T. Ryan, Analysis of the assembly profiles for mitochondrial- and nuclear-DNA-encoded subunits into complex I, Mol. Cell Biol. 27 (2007) 4228–4237.

[48] D.A. Stroud, E.E. Surgenor, L.E. Formosa, B. Reljic, A.E. Frazier, M.G. Dibley, L. D. Osellame, T. Stait, T.H. Beilharz, D.R. Thorburn, A. Salim, M.T. Ryan, Accessory subunits are integral for assembly and function of human mitochondrial complex I, Nature 538 (2016) 123–126.

[49] E. Mick, D.V. Titov, O.S. Skinner, R. Sharma, A.A. Jourdain, V.K. Mootha, Distinct mitochondrial defects trigger the integrated stress response depending on the metabolic state of the cell, Elife 9 (2020), e49178.

[50] C.T.J. Wall, G. Lefebvre, S. Metairon, P. Descombes, A. Wiederkehr, J. Santo-Domingo, Mitochondrial respiratory chain dysfunction alters ER sterol sensing and mevalonate pathway activity, J. Biol. Chem. 298 (2022), 101652.

[51] X.R. Bao, S.-E. Ong, O. Goldberger, J. Peng, R. Sharma, D.A. Thompson, S.B. Vafai, A.G. Cox, E. Marutani, F. Ichinose, W. Goessling, A. Regev, S.A. Carr, C.B. Clish, V. K. Mootha, Mitochondrial dysfunction remodels one-carbon metabolism in human cells, Elife 5 (2016), e10575.

[52] S. Ahola, P. Rivera Mejías, S. Hermans, S. Chandragiri, P. Giavalisco, H. Nolte, T. Langer, OMA1-mediated integrated stress response protects against ferroptosis in mitochondrial cardiomyopathy, Cell Metabol. S1550–4131 (22) (2022) 360–366.

[53] N.A. Khan, J. Nikkanen, S. Yatsuga, C. Jackson, L. Wang, S. Pradhan, R. Kivelä, A. Pessia, V. Velagapudi, A. Suomalainen, mTORC1 regulates mitochondrial integrated stress response and mitochondrial myopathy progression, Cell Metabol. 26 (2017) 419–428.e5.

[54] J. Nikkanen, S. Forsström, L. Euro, I. Paetau, R.A. Kohnz, L. Wang, D. Chilov, J. Viinamäki, A. Roivainen, P. Marjamäki, H. Liljenbäck, S. Ahola, J. Buzkova, M. Terzioglu, N.A. Khan, S. Pirnes-Karhu, A. Paetau, T. Lönnqvist, A. Sajantila, P. Isohanni, H. Tyynismaa, D.K. Nomura, B.J. Battersby, V. Velagapudi, C. J. Carroll, A. Suomalainen, Mitochondrial DNA replication defects disturb cellular dNTP pools and remodel one-carbon metabolism, Cell Metabol. 23 (2016) 635–648.

[55] R. Acín-Pérez, M.P. Bayona-Bafaluy, P. Fernández-Silva, R. Moreno-Loshuertos, A. Pérez-Martos, C. Bruno, C.T. Moraes, J.A. Enríquez, Respiratory complex III is required to maintain complex I in mammalian mitochondria, Mol. Cell 13 (2004) 805–815.

[56] B.P. Tu, J.S. Weissman, The FAD- and O(2)-dependent reaction cycle of Ero1-mediated oxidative protein folding in the endoplasmic reticulum, Mol. Cell 10 (2002) 983–994.

[57] B.V. O'Donnell, D.G. Tew, O.T. Jones, P.J. England, Studies on the inhibitory mechanism of iodonium compounds with special reference to neutrophil NADPH oxidase, Biochem. J. 290 (Pt 1) (1993) 41–49.

[58] M.-Z. Peng, Y.-X. Shao, X.-Z. Li, K.-D. Zhang, Y.-N. Cai, Y.-T. Lin, M.-Y. Jiang, Z.-C. Liu, X.-Y. Su, W. Zhang, X.-L. Jiang, L. Liu, Mitochondrial FAD shortage in SLC25A32 deficiency affects folate-mediated one-carbon metabolism, Cell. Mol. Life Sci. 79 (2022) 375.

[59] A.N. Spaan, L. Ijlst, C.W.T. van Roermund, F.A. Wijburg, R.J.A. Wanders, H. R. Waterham, Identification of the human mitochondrial FAD transporter and its potential role in multiple acyl-CoA dehydrogenase deficiency, Mol. Genet. Metabol. 86 (2005) 441–447.

[60] T.A. Giancaspero, M. Galluccio, A. Miccolis, P. Leone, I. Eberini, S. Iametti, C. Indiveri, M. Barile, Human FAD synthase is a bi-functional enzyme with a FAD hydrolase activity in the molybdopterin binding domain, Biochem. Biophys. Res. Commun. 465 (2015) 443–449.

[61] A.B. Kotlyar, J.S. Karliner, G. Cecchini, A novel strong competitive inhibitor of complex I, FEBS Lett. 579 (2005) 4861–4866.

[62] T.V. Zharova, A.D. Vinogradov, A competitive inhibition of the mitochondrial NADH-ubiquinone oxidoreductase (complex I) by ADP-ribose, Biochim. Biophys. Acta 1320 (1997) 256–264.

[63] L.G. Iacovino, J. Reis, A. Mai, C. Binda, A. Mattevi, Diphenylene iodonium is a noncovalent mao inhibitor: a biochemical and structural analysis, ChemMedChem 15 (2020) 1394–1397.

[64] D.G. Tew, Inhibition of cytochrome P450 reductase by the diphenyliodonium cation. Kinetic analysis and covalent modifications, Biochemistry (Mosc.) 32 (1993) 10209–10215.

[65] J. Doussière, P.V. Vignais, Diphenylene iodonium as an inhibitor of the NADPH oxidase complex of bovine neutrophils. Factors controlling the inhibitory potency of diphenylene iodonium in a cell-free system of oxidase activation, Eur. J. Biochem. 208 (1992) 61–71.

[66] V.D. Sled, A.D. Vinogradov, Reductive inactivation of the mitochondrial three subunit NADH dehydrogenase, Biochim. Biophys. Acta 1143 (1993) 199–203.

[67] A. Stepanova, S. Sosunov, Z. Niatsetskaya, C. Konrad, A.A. Starkov, G. Manfredi, I. Wittig, V. Ten, A. Galkin, Redox-dependent loss of flavin by mitochondrial complex I in brain ischemia/reperfusion injury, Antioxidants Redox Signal. 31 (2019) 608–622.

[68] P.J. Holt, R.G. Efremov, E. Nakamaru-Ogiso, L.A. Sazanov, Reversible FMN dissociation from Escherichia coli respiratory complex I, Biochim. Biophys. Acta 1857 (2016) 1777–1785.

[69] I.S. Gostimskaya, V.G. Grivennikova, G. Cecchini, A.D. Vinogradov, Reversible dissociation of flavin mononucleotide from the mammalian membrane-bound NADH: ubiquinone oxidoreductase (complex I), FEBS Lett. 581 (2007) 5803–5806.

[70] M.G. Dibley, L.E. Formosa, B. Lyu, B. Reljic, D. McGann, L. Muellner-Wong, F. Kraus, A.J. Sharpe, D.A. Stroud, M.T. Ryan, The mitochondrial acyl-carrier protein interaction network highlights important roles for LYRM family members in complex I and mitoribosome assembly, Mol. Cell. Proteomics 19 (2020) 65–77.

[71] K.R. Pryde, J.W. Taanman, A.H. Schapira, A LON-ClpP proteolytic Axis degrades complex I to extinguish ROS production in depolarized mitochondria, Cell Rep. 17 (2016) 2522–2531.

[72] P.M. Quirós, Y. Español, R. Acín-Pérez, F. Rodríguez, C. Bárcena, K. Watanabe, E. Calvo, M. Loureiro, M.S. Fernández-García, A. Fueyo, J. Vázquez, J.A. Enríquez, C. López-Otín, ATP-dependent Lon protease controls tumor bioenergetics by reprogramming mitochondrial activity, Cell Rep. 8 (2014) 542–556.

[73] E. Fassone, A.J. Duncan, J.-W. Taanman, A.T. Pagnamenta, M.I. Sadowski, T. Holand, W. Qasim, P. Rutland, S.E. Calvo, V.K. Mootha, M. Bitner-Glindzicz, S. Rahman, FOXRED1, encoding an FAD-dependent oxidoreductase complex-I-specific molecular chaperone, is mutated in infantile-onset mitochondrial encephalopathy, Hum. Mol. Genet. 19 (2010) 4837–4847.

[74] J. Nouws, L. Nijtmans, S.M. Houten, M. van den Brand, M. Huynen, H. Venselaar, S. Hoefs, J. Gloerich, J. Kronick, T. Hutchin, P. Willems, R. Rodenburg, R. Wanders, L. van den Heuvel, J. Smeitink, R.O. Vogel, Acyl-CoA dehydrogenase 9 is required for the biogenesis of oxidative phosphorylation complex I, Cell Metabol. 12 (2010) 283–294.

[75] P. Roestenberg, G.R. Manjeri, F. Valsecchi, J.A.M. Smeitink, P.H.G.M. Willems, W. J.H. Koopman, Pharmacological targeting of mitochondrial complex I deficiency: the cellular level and beyond, Mitochondrion 12 (2012) 57–65.

[76] M. Barile, C. Brizio, D. Valenti, C. De Virgilio, S. Passarella, The riboflavin/FAD cycle in rat liver mitochondria, Eur. J. Biochem. 267 (2000) 4888–4900.

[77] S.A. Titus, R.G. Moran, Retrovirally mediated complementation of the glyB phenotype. Cloning of a human gene encoding the carrier for entry of folates into mitochondria, J. Biol. Chem. 275 (2000) 36811–36817.
[78] M. Schiff, A. Veauville-Merllié, C.H. Su, A. Tzagoloff, M. Rak, H. Ogier de Baulny, A. Boutron, H. Smedts-Walters, N.B. Romero, O. Rigal, P. Rustin, C. Vianey-Saban, C. Acquaviva-Bourdain, SLC25A32 mutations and riboflavin-responsive exercise intolerance, N. Engl. J. Med. 374 (2016) 795–797.
[79] T.S. Luongo, J.M. Eller, M.-J. Lu, M. Niere, F. Raith, C. Perry, M.R. Bornstein, P. Oliphint, L. Wang, M.R. McReynolds, M.E. Migaud, J.D. Rabinowitz, F. B. Johnson, K. Johnsson, M. Ziegler, X.A. Cambronne, J.A. Baur, SLC25A51 is a mammalian mitochondrial NAD+ transporter, Nature 588 (2020) 174–179.
[80] N. Kory, J. Uit de Bos, S. van der Rijt, N. Jankovic, M. Güra, N. Arp, I.A. Pena, G. Prakash, S.H. Chan, T. Kunchok, C.A. Lewis, D.M. Sabatini, MCART1/SLC25A51 is required for mitochondrial NAD transport, Sci. Adv. 6 (2020), eabe5310.
[81] E. Girardi, G. Agrimi, U. Goldmann, G. Fiume, S. Lindinger, V. Sedlyarov, I. Srndic, B. Gürtl, B. Agerer, F. Kartnig, P. Scarcia, M.A. Di Noia, E. Liñeiro, M. Rebsamen, T. Wiedmer, A. Bergthaler, L. Palmieri, G. Superti-Furga, Epistasis-driven identification of SLC25A51 as a regulator of human mitochondrial NAD import, Nat. Commun. 11 (2020) 6145.
[82] Y. Wang, F.S. Yen, X.G. Zhu, R.C. Timson, R. Weber, C. Xing, Y. Liu, B. Allwein, H. Luo, H.-W. Yeh, S. Heissel, G. Unlu, E.R. Gamazon, M.G. Kharas, R. Hite, K. Birsoy, SLC25A39 is necessary for mitochondrial glutathione import in mammalian cells, Nature 599 (2021) 136–140.
[83] X. Shi, B. Reinstadler, H. Shah, T.-L. To, K. Byrne, L. Summer, S.E. Calvo, O. Goldberger, J.G. Doench, V.K. Mootha, H. Shen, Combinatorial GxGxE CRISPR screen identifies SLC25A39 in mitochondrial glutathione transport linking iron homeostasis to OXPHOS, Nat. Commun. 13 (2022) 2483.